EXPERIMENTAL INVESTIGATION OF A BUOYANT JET

by

A. Rahim A. Munshi

A thesis submitted to the Faculty
of the Graduate School of State University
of New York at Buffalo in partial fulfillment
of the requirements for the degree of
Master of Science

February 1981

TABLE OF CONTENTS

ACKNOWLEDGEMENTS

The author wishes to acknowledge all the help and guidance given by Dr. William K. George, Professor in Mechanical and Aerospace Engineering, during the completion of this thesis.

I also wish to express many thanks to my family, especially to my mother, who has done everything for building my career.

Special thanks to Dr. C. Bruce Baker, Assistant Professor at the University of Pittsburgh at Johnstown for immediately taking over the advisory work and helping me complete the last stages of this thesis in the absence of Dr. W. K. George. Last but not least, thanks to Mrs. Eileen Graber for typing the manuscript.

This research was supported by the Atmospheric Science Division, National Science Foundation under grants No. ATM 7601257 and ATM 7923729.

LIST OF FIGURES

LIST OF FIGURES (cont.)

Nomenclature

d	Diameter of the hot wire sensor
D	Diameter of the nozzle
E_T	Output voltage of the Temperature Anemometer
e_T	Fluctuating part of E_T
E_u	Output voltage of the Velocity Anemometer
e_u	Fluctuating part of E_u
F_o	Buoyancy
$f(\eta)$	Similarity function for the mean axial velocity
G	Amplifier gain
g	Acceleration due to gravity
$h(\eta)$	Similarity function for Reynolds stress
I	Current through hot wire
K	Thermal conductivity
$k(\eta)$	Similarity function for the radial velocity
L	Forced length scale
ℓ	Hot wire length
M	Momentum
Nu	Nusselt number
$p(\eta)$	Similarity function for the mean temperature difference
Q	Flowrate
$q(\eta)$	Similarity function for the radial turbulent heat flux
Re	Reynolds number
R_w	Resistance of the hot wire sensor
r	Radial coordinate
T	Local temperature
T_f	Film temperature

Nomenclature (cont.)

T_w	Temperature of the hot wire sensor
T_∞	Ambient temperature
ΔT	Local and ambient temperature difference
t	Temperature fluctuations
U	Mean axial velocity
u	Axial velocity fluctuations
V	Mean radial velocity
v	Radial velocity fluctuations
X	Axial coordinate
β	Coefficient of thermal expansion
ξ	Dimensionless length
η	Dimensionless radial coordinate
ν	Kinematic viscosity
ρ	Density
ρ_∞	Ambient air density
$\Delta\rho$	Local and ambient density difference
τ	Time
b	Width parameter for entrainment function
A	A constant

ABSTRACT

The investigation consists of a detailed experimental study of an axisymmetric turbulent buoyant jet in a uniform environment. The jet is generated with various Froude numbers,and data are obtained at various positions with the help of a traverser mechanism. The measurement techniques use hot wire anemometry methods to produce instantaneous velocity and temperature signals. A two wire probe is used and measurements are taken at various locations of x/D = 31.5, 39 and 47.2.

A polynomial relating Reynolds numbers and Nusselt numbers is fitted to the velocity calibration data and gives a good collapse of the data for various flow conditions encountered. The profiles of mean and R.M.S. velocities and temperature and their correlations, normalized by similarity variables, are presented. Also, the total buoyancy flux and the contribution to the flux by the turbulence are estimated.

The measured mean velocity and temperature profiles are compared with available theory. These comparisons are reasonable.

1. INTRODUCTION

1.1 Buoyant Jet

A jet is defined as a flow which is driven by the continuous addition of momentum at the source whereas a plume is defined as a flow which is driven by the continuous addition of buoyancy at the source. If both buoyancy and momentum are continuously added at the source, the flow is called a buoyant jet. Even if the rate at which momentum is added at the source is sufficiently large to dominate the effect of the buoyancy discharge so that the flow is jet-like, it will eventually evolve into a plume-like flow since the initial buoyancy (no matter how small) continuously produces additional momentum. Consequently the jet and plume represents the limits of a buoyant jet.

A set of dimensionless equations is available which describes the mean velocity and temperature (buoyancy) profiles for the buoyant jet as it evolves from a jet to a plume. These equations depend on two dimensionless coordinates, η and ξ, defined and explained in the later sections.

1.2 Background

The study of turbulent buoyant jets is rather recent. The problem was first addressed by Morton (13) in 1959. Studies of the asixymmetric turbulent jet were undertaken in the 1920's. In 1926 Tollmien (17) developed a theoretical analysis for turbulent jet flow using Prandtl's mixing length theory. Görtler (18) developed the eddy viscosity model for jet flow in 1942. Early measurements of the jet mean velocities and temperatures include work by Zimm (19), Ruden (20), Reichart (21), Hinze and Van Der Hegge Zignen (22) and Corrsin and Uberoi (23).

The data for axisymmetric buoyant jets are extremely scarce, but measurements of centerline temperatures and mean temperature profiles have been

made. These include measurements by Abraham (24), Kotsovinos and List (25), Ryskiewich and Hafetz (26) and Pryputniewicz (27). Velocity measurements for the buoyant jet region are even more scarce.

1.3 Integral Techniques

After the introduction of the similarity analysis developed independently by Zel'dovich (16), Batchelor (3) and Rouse et al. (12), integral methods were the only techniques used to model buoyant jet and plume flows until the 1970's. The suggested similarity solutions assumed the form

$$U = F_o^{1/3} x^{-1/3} f(\eta) \tag{1.3.1}$$

$$g\beta\Delta T = F_o^{2/3} x^{-5/3} t(\eta) \tag{1.3.2}$$

$$\eta = r/x \tag{1.3.3}$$

$$b = Ax \tag{1.3.4}$$

Morton et al.(13) used these parameters in the integral forms of the mean flow equations to develop a model to describe plumes. The integral equations take the following forms:

$$\frac{d}{dx}(b^2U) = 2\alpha bU \tag{1.3.5}$$

$$\frac{d}{dx}(b^2U^2) = b^2 g \frac{\rho_o - \rho}{\rho_1} \tag{1.3.6}$$

$$\frac{d}{dx}\left(b^2 U g \frac{\rho_o - \rho}{\rho}\right) = b^2 \frac{Ug}{\rho_1} \frac{d\rho_o}{dx} \quad , \tag{1.3.7}$$

Equation (1.3.5) results from the integration of the continuity equations and the so called "entrainment hypothesis", in which it is assumed that the radial velocity $\overline{V}_\infty$ is proportional to the mean axial velocity $\overline{U}$. This assumption is evident in the appearance of the entrainment coefficient α. Equations (1.3.6) and (1.3.7) are the results of the integration of the momentum and buoyancy (or temperature) equations. A solution of this system of equations requires that the entrainment coefficient be known.

Morton et al.(13) applied this technique to plumes in neutral and stratified environments. Morton extended this work to include forced plumes (or buoyant jets) by assuming that the entrainment coefficient was the same for both jets and plumes and thus constant throughout the entire flow field. This work remains the standard for most engineering analysis.

The assumption that the entrainment coefficient was constant from jet to plume was shown to be incorrect and inconsistent with experiment by List and Imberger (28). The experimenters developed an approximation of how the entrainment coefficient α should vary as a buoyant jet becomes a plume by using an empirical model for α which behaved properly in the limits. The development by List and Imberger (28) has been extended by Kotsovinos (25). This conclusion is also supported in the theoretical analyses of Baker (9).

1.4 Scaling Techniques

A set of dimensionless equations which describe the mean velocity and temperature (buoyancy) profiles for buoyant jet as it evolves from a jet to a plume has been developed by Baker (9). These equations depend on two dimensionless coordinates, η and ξ, defined by

$$\eta = r/x \tag{1.4.1}$$

and

$$\xi = x/L \tag{1.4.2}$$

where L is a new characteristic length scale (the "forced" length scale) defined by the rate at which buoyancy and momentum are added at the source:

$$L = M_o^{3/4}/F_o^{1/2} \tag{1.4.3}$$

The length scale L is obtained from dimensionless arguments based on the momentum and energy integrals. These integrals are:

$$M_o = 2\pi \int_o^\infty U^2 \, r dr \tag{1.4.4}$$

$$F_o = 2\pi \int_o^\infty U g \beta \Delta T \, r dr \tag{1.4.5}$$

with dimensions

$$M_o = [\frac{L^4}{T^2}] \tag{1.4.6}$$

$$F_o = [\frac{L^4}{T^3}] \tag{1.4.7}$$

Consequently, the ratio $M_o^{3/4}/F_o^{1/2}$ has units of length (L).

The mean equations for momentum, temperature and mass conservation in reduced form for a fully developed, axisymmetric hot turbulent jet discharging vertically into a constant temperature (neutral) environment

of infinite extent, as shown in the figure (1-1), are

$$U \frac{\partial U}{\partial x} + V \frac{\partial U}{\partial r} = \frac{1}{r} \frac{\partial}{\partial r} (-r \overline{uv}) + g\beta\Delta T \qquad (1.4.8)$$

$$U \frac{\partial \Delta T}{\partial x} + V \frac{\partial \Delta T}{\partial r} = \frac{1}{r} \frac{\partial}{\partial r} (-r \overline{v\theta}) + \frac{\partial}{\partial x} (\overline{-u\theta}) \qquad (1.4.9)$$

$$\frac{\partial U}{\partial x} + \frac{1}{r} \frac{\partial}{\partial r} (rV) = 0 \quad . \qquad (1.4.10)$$

In these equations the Boussinesq approximations are employed and the molecular diffusion of momentum and heat is assumed negligible relative to the transport of these quantities by the turbulence. Both the momentum and temperature equations can be integrated across the flow to yield the integral equations used by previous investigators. These are:

Momentum:

$$\frac{d}{dx} \int_0^\infty U^2 \, rdr = \int_0^\infty g\beta\Delta T \, rdr \qquad (1.4.11)$$

Temperature: (Buoyancy)

$$\int_0^\infty g\beta\Delta T \, U \, rdr = \frac{F_o}{2\pi} \quad . \qquad (1.4.12)$$

The initial condition for the momentum integral equation is

$$\int_0^\infty U^2 \, rdr = \frac{M_o}{2\pi} \, ,$$

which is the rate at which momentum is discharged at the source.

Equations 1.4.8 through 1.4.12 have been reduced to dimensionless forms by Baker (9) using the transforms

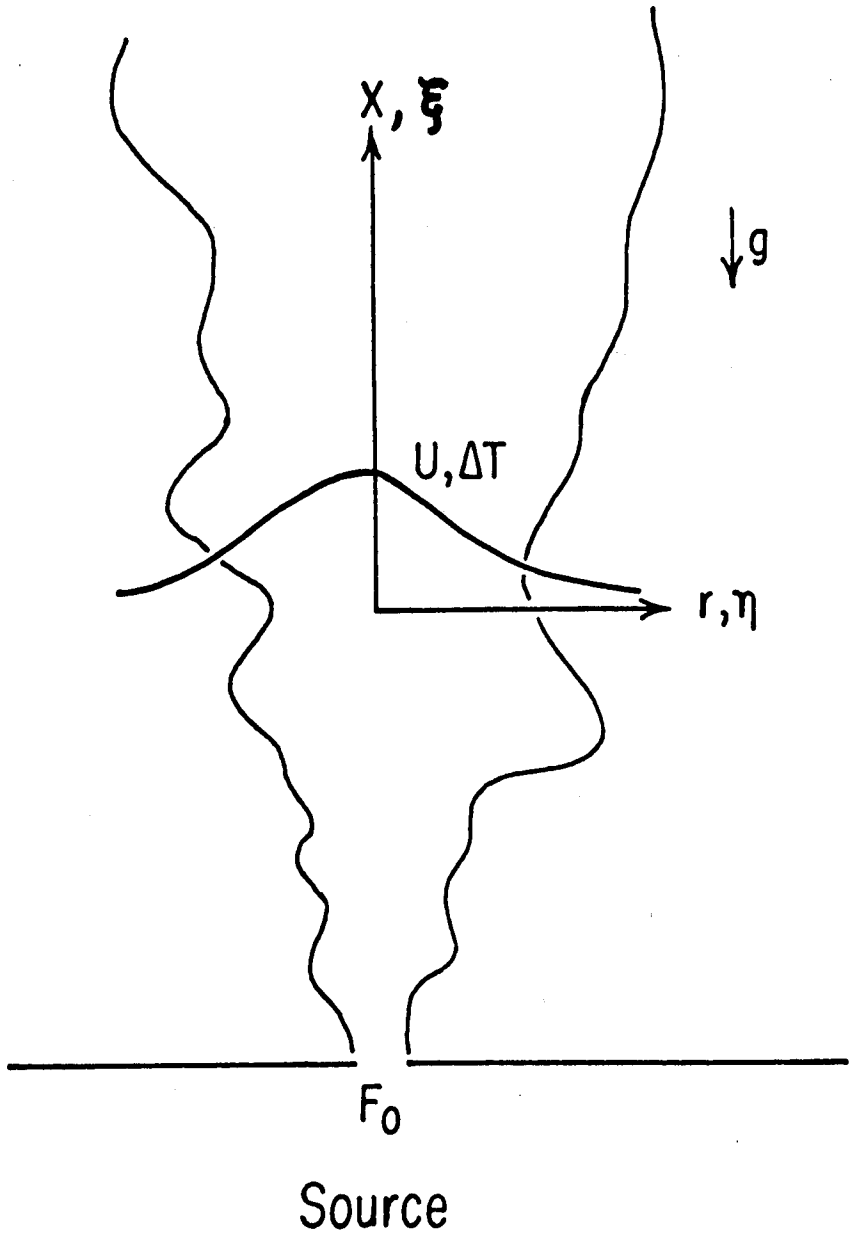

Figure (1-1) Jet Coordinates

$$\eta = r/x$$

$$\xi = x/L$$

$$U = M_o^{1/2} x^{-1} f(\eta,\xi)$$

$$V = M_o^{1/2} x^{-1} k(\eta,\xi)$$

$$\overline{uv} = M_o x^{-2} S(\eta,\xi)$$

$$g\beta\Delta T = F_o M_o^{-1/2} x^{-1} t(\eta,\xi)$$

$$g\beta\overline{v\theta} = F_1 x^{-2} h(\eta,\xi) \ .$$

Applying these transforms to equations 1.4.8 through 1.4.12 and ignoring the vertical heat flux term $\overline{u\theta}$ yields

$$f^2 + \frac{f'}{\eta}\int_o^\eta f\,\eta d\eta - \frac{(\eta s)'}{\eta} = -\xi^2 t + \xi[f\frac{\partial f}{\partial \xi} - \frac{f'}{\eta}\int_o^\eta \frac{\partial f}{\partial \xi}\,\eta d\eta] \qquad (1.4.13$$

$$tf + \frac{t'}{\eta}\int_o^\eta f\,\eta d\eta - \frac{(\eta h)'}{\eta} = \xi[f\,\frac{\partial t}{\partial \xi} - \frac{t'}{\eta}\int_o^\eta \frac{\partial f}{\partial \eta}\,\eta d\eta] \qquad (1.4.14$$

$$\frac{d}{d\xi}\int_o^\infty f^2\,\eta d\eta = \xi\int_o^\infty t\,\eta d\eta \qquad (1.4.15$$

$$\int_o^\infty f\,t\,\eta d\eta = \frac{1}{2\pi} \ . \qquad (1.4.16$$

It should be noted in equation 1.4.13 that the buoyancy term t is controlled by ξ^2, i.e. as $\xi \to o$ buoyancy effects disappear and as $\xi \to \infty$ buoyancy effects dominate the flow. Thus the ξ parameter is a measure of whether the flow is a jet, a buoyant jet or a plume.

2. DESCRIPTION OF EXPERIMENTAL APPARATUS, PROCEDURE AND MEASURING TECHNIQUES.

2.1 The Plume Facility

The plume facility is located in a large room (5000 sq. ft.) with a ceiling height of 24 ft. The facility consists of a large, square, steel structure (6' x 6' x 20') which is wrapped in 4 mil plastic to prevent cross drafts. The interior of this enclosure has three sections of window screening to prevent unwanted circulation - each two or three layers in thickness. A sketch of the entire facility is presented in Figure (2.1).

The plume is generated by passing compressed air through an insulated electric heater placed at the base of the steel structure. The heater is described in detail in Figure (2.2). Before entering the heater the air is filtered and the mass flow rate is measured with a calibrated rotometer. The air enters at the base of the heater and passes through a section of sintered bronze containing resistance heating elements. The air then passes through two screens and a 15:1 contraction ratio to exit into the ambient air. The exit temperature can be raised in excess of 300°C and maintained at a constant temperature with an Electromax Controller connected to an SCR power supply. The exit profiles of velocity and temperature are flat to within 2%. Since both the mass flow rates and the heat flux are variable, it is possible to create exit conditions with Froude numbersof different magnitudes. The heater has an output capability of 3000 watts.

Air for entrainment is fed to the base of the heater, rises between the plastic and outer layers of screening, and is entrained radially inward through the screens. The distance between the plastic and the outer screen is roughly 6 to 8 inches. This outer screen is 2 to 3 layers thick and

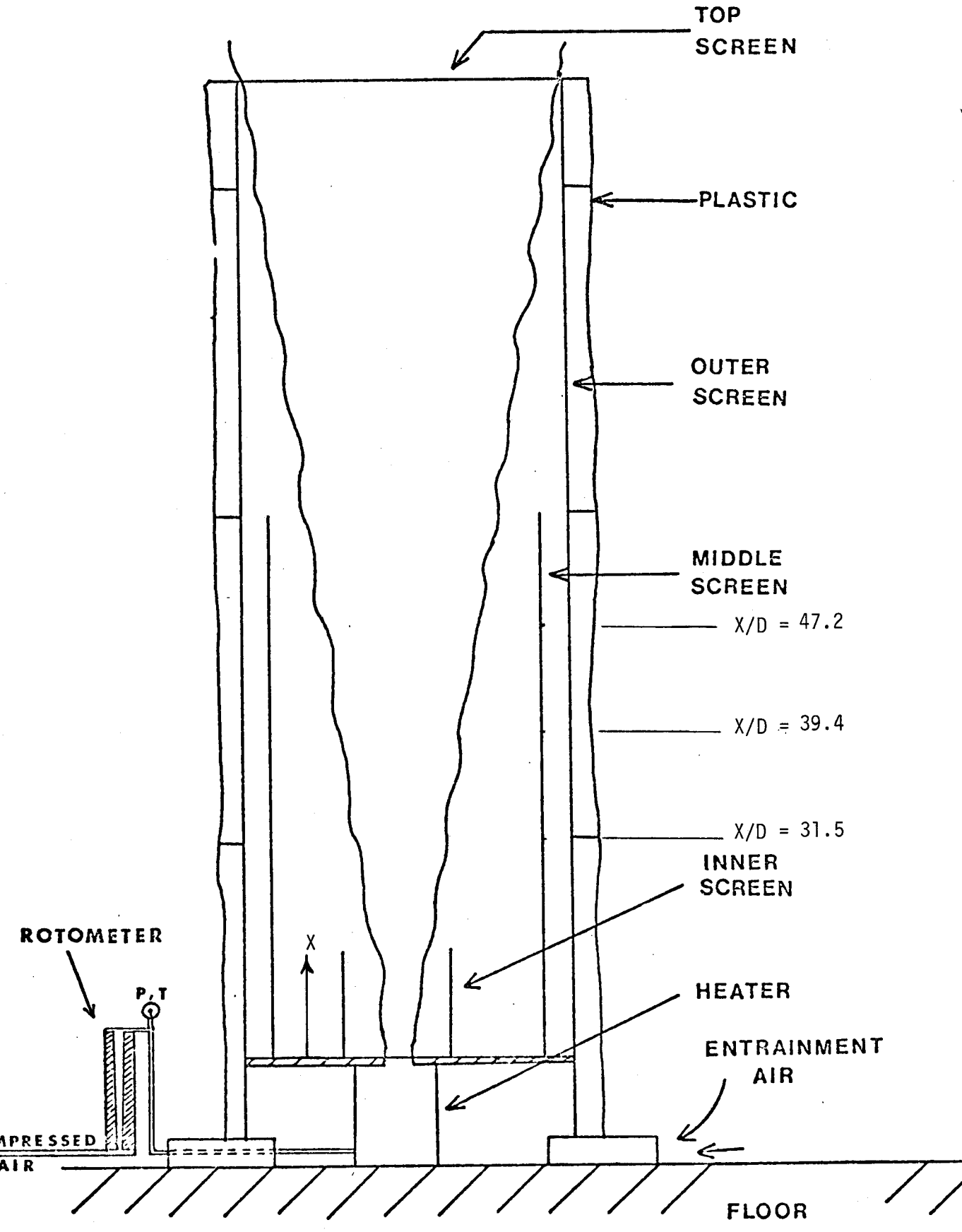

Figure (2-1) Jet Facility

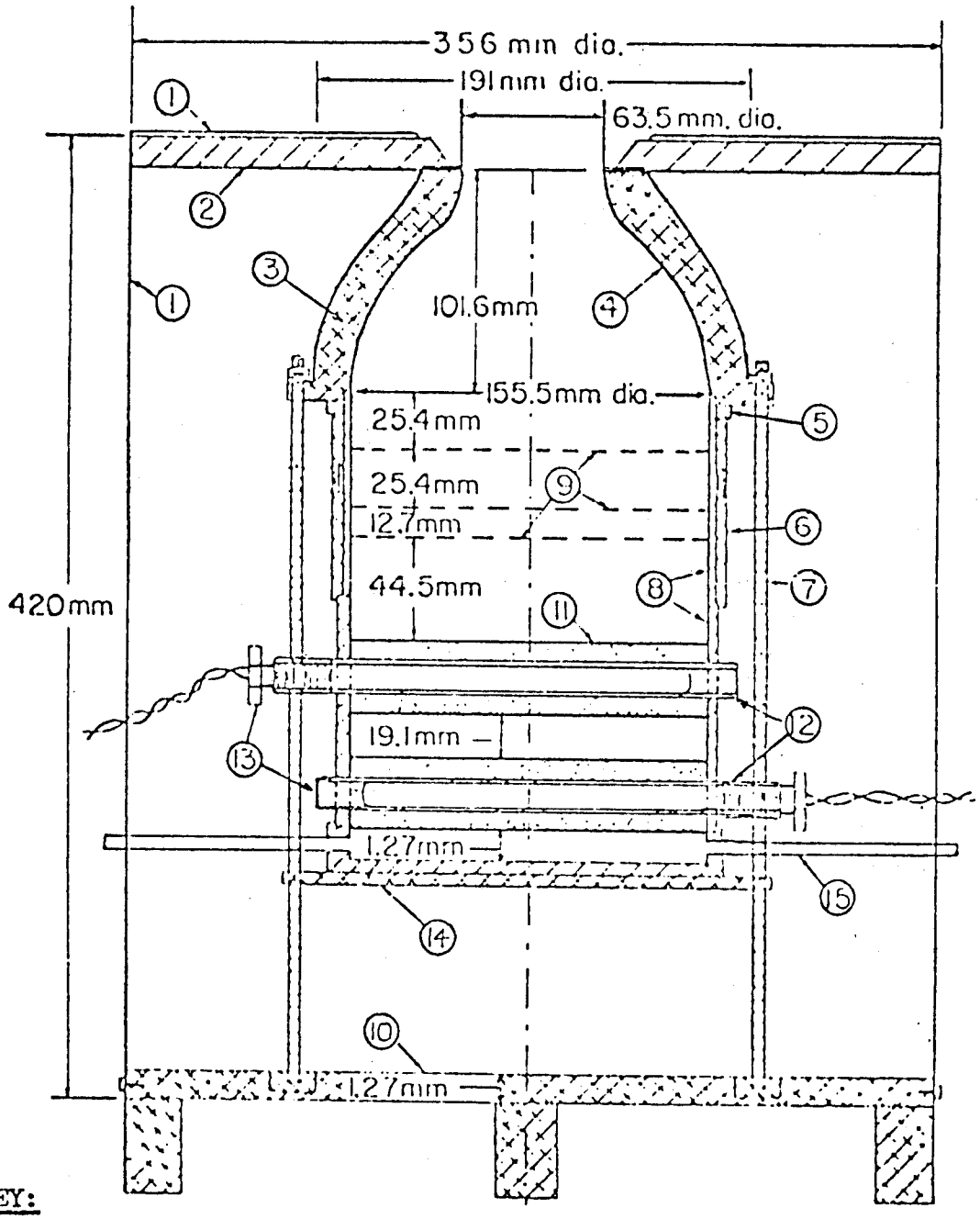

KEY:

(1) Container for silica aerogel insulation, sheet steel. (2) Cerafelt insulation. (3) Aluminum exit nozzle. (4) inner surface; Radius (mm.) = 51.75 + 2.42E-08 x^5 - 6.1E-06 x^4 + 4.36E-04 x^3. (5) Gasket. (6) Bronze sleeve. (7) Three threaded rods spaced 120° apart. (8) Copper spacer. (9) Stainless steel screens; 1.18 wires/mm.,0.305 mm. dia. (10) Aluminum base plate. (11) Two sintered bronze castings; density 5 g/cm^3, smallest passage 150 um. (12) Eight copper pipes; top four positioned perpendicular to bottom four. (13) Eight electric heaters; Watlow Firerod C6A81, 400 W. each. (14) Bronze base plate. (15) Four air inlet pipes, 90° apart.

Figure (2-2) Plume Calibrator

rises the full height of 20 ft. The middle layer of screening is octagonally shaped (and is more closely tailored to the shape of the buoyant jet) and has a diameter of roughly 5 ft., extending only 8 ft. in height. Most of the measurements are taken in this section. The innermost layer of screening is circular in shape, 1-1/2 ft. in height, and has a 2 ft. diameter

2.2 Calibration Technique and Procedure

The velocity and temperature wires are calibrated at the exit of the plume source at several velocities and temperatures. The exit temperature or the reference temperature is obtained from a copper-constantan thermocouple placed near the sensor, and the velocity reference is determined by applying mass conservation to the reading of the upstream rotometer. Since the air temperature changes as it passes through the heater, its upstream properties must be measured. This is accomplished with a manometer and a thermometer placed at the exit of the rotometer. The rotometer was calibrated by measuring the output velocity of the plume source with a laser Doppler anemometer.

The velocity sensor calibration is accomplished by converting the anemometer voltage and flow velocity to Nusselt number and Reynolds number as defined by equation

$$R_d = \frac{\overline{U}_o\, d}{\nu} \tag{2.2.1}$$

$$Nu = \frac{I^2 R_w}{\pi L K\,(T_w - T_g)} \tag{2.2.2}$$

where

T_w is the wire temperature

T_g is the gas temperature

d is the wire diameter

L is the wire length

R_w is the wire resistance

and k is the thermal conductivity of the gas.

A polynomial of the forms of equations (2.2.3) is then fitted to this data.

$$R_d = A_0 + A_1 Nu^{1/2} + A_2 Nu + A_3 Nu^{3/2} + A_4 Nu^2 \qquad (2.2.3)$$

One parameter that was difficult to measure was the sensor resistance. Because there was no way of shorting the probe across the sensor without fear of breakage, this parameter was adjusted after the calibration to give the best collapse of the data for all temperatures. The Reynolds number was evaluated at the local gas temperature and Nusselt number at the film temperature ($T_{film} = \frac{T_{gas} + T_{wire}}{2}$). This gives a good collapse of the data for the working Reynolds number range. Also the polynomial type equation used to fit the data was chosen for ease of calculation by a computer.

The temperature sensor is calibrated at the same time as the velocity sensor. The temperature sensor wire is operated at a low current. Consequently, the sensitivity of the wire to velocity is negligible and the calibration equation reduced to a linear expression as shown

$$T = C_1 + C_2 E_t \qquad (2.2.4)$$

The velocity and temperature anemometer voltages are indicated on DC voltmeters. The flowmeter was calibrated from 60 CFH - 720 CFH, which covers the range of velocities (0.6 m/s - 7.2 m/s) encountered in this experiment. The flow temperature is varied from 27°C to 52°C, which

corresponds to the range of flow conditions encountered.

Two computer programs, namely WIRECAL and CURFIT, are used to curve fit the velocity and temperature calibration data. The temperature and velocity calibration curves are shown in figures (2-3) and (2-4) respectively. Since it is very difficult to measure the wire resistance, the parameter $\Delta R/\Delta T$ used in programs CURFIT is varied slightly to get the best possible collapse of the data.

2.3 Experimental Procedure

The jet was operated at Froude numbers which were accomplished by changing both the flow and temperature. The higher velocities and flow rates were achieved by reducing the exit nozzle diameter to 3.175 cms and using a high capacity flowmeter in the air line. Those changes provided a maximum flow rate of 1500 ft^3/hr, exit velocities up to 14 m/s.

The experiment consists of two different sets of data acquired at two different Froude numbers, namely, 10.74 and 22.06, these were achieved by setting exit conditions of velocities and temperatures as 300 $ft^3/hr.$, 563°k and 600 $ft^3/hr.$, 483°k.

Because of the limitations in the capacity of the heaters and temperature controller, the maximum temperature attained was 483°k at a flow velocity of 9.6 m/s. The exit temperature was constant to $\pm$°1 during the test run. The ambient stratification was greatly reduced by modifying the outermost top plastic covering around the plume. The resulting stratification was 0.75°F over a height of 2 meters for a time period of 5 hours.

To achieve thermal equilibrium for the nozzle and the heater walls, the plume was operated for at least 5-6 hours before the measurements were taken. Measurements were taken at various values of $\eta = r/x$ with a spacing

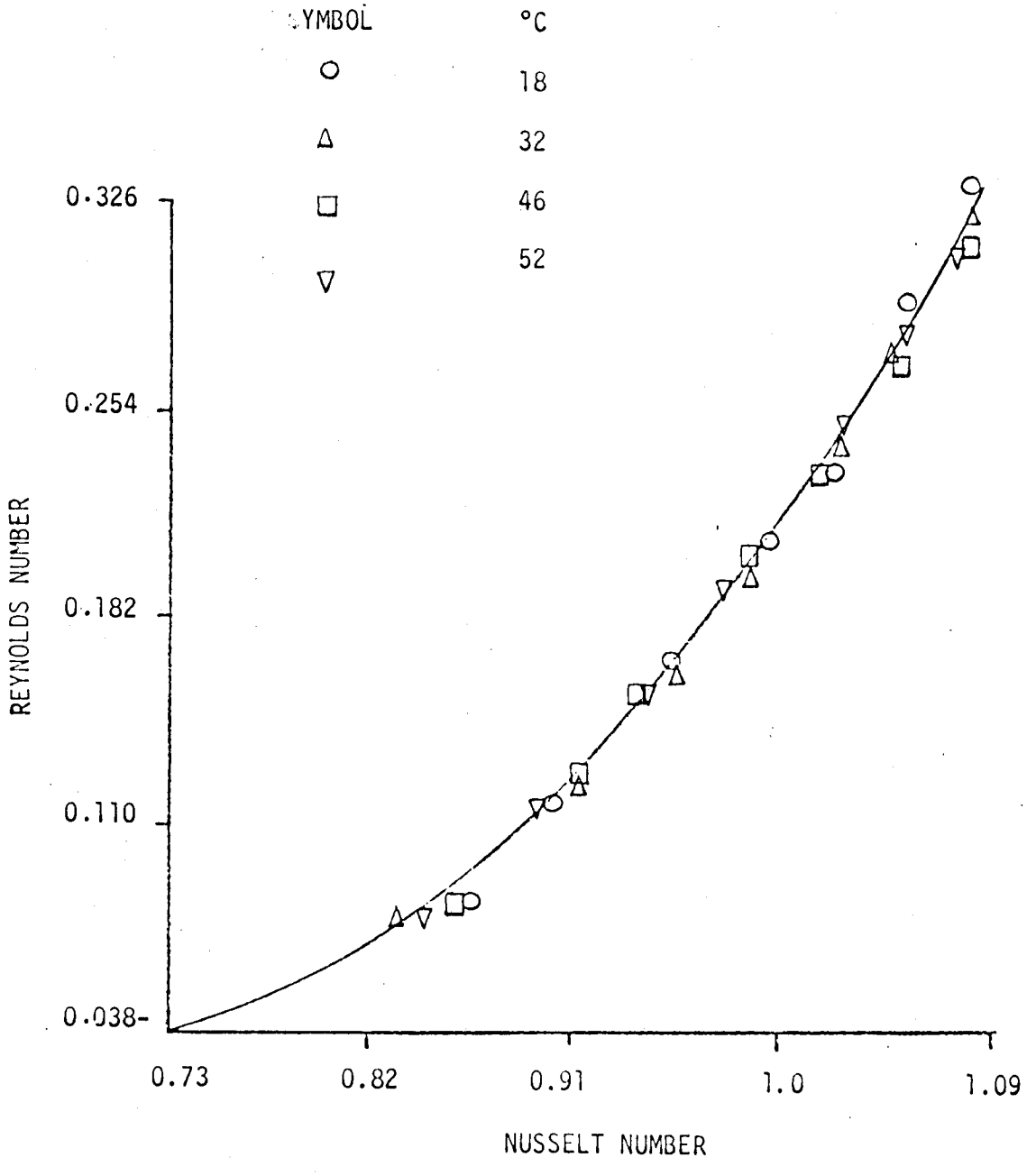

Figure (2-3) Velocity Calibration Data

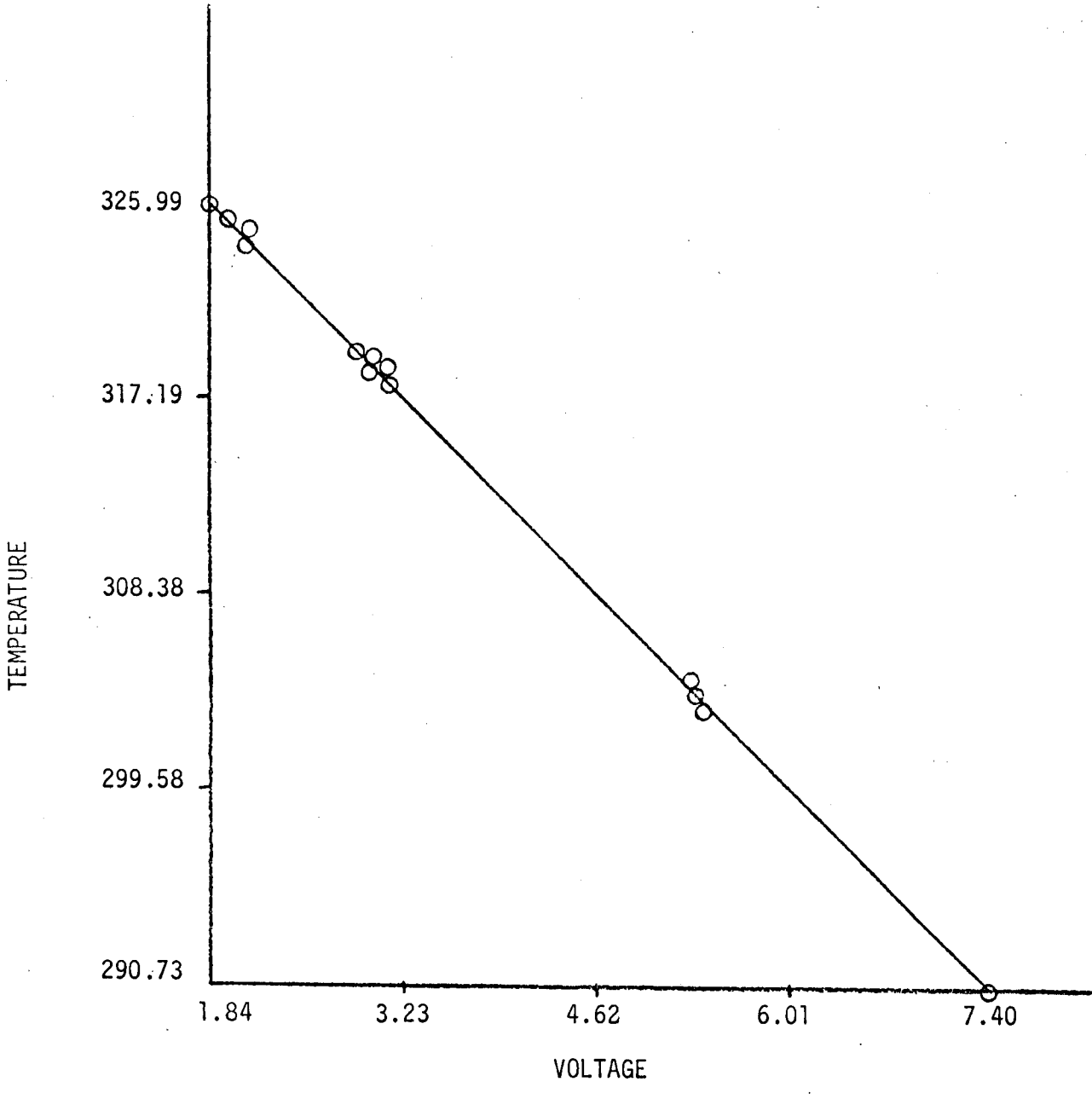

Figure (2-4) Temperature Calibration Data

of $\Delta\eta = 0.025$ between points. The actual displacement from the center varies with the height, and the vertical locations correspond to x/D of 31.5, 39.4, a 47.2 respectively. The horizontal and vertical movement was achieved by a traverser mechanism.

2.4 Data Acquisition

The mean velocity-like and temperature-like signals (i.e. $\overline{E_u}$ and $\overline{E_T}$) are directly recorded from D.C. voltmeters. R.M.S. velocity-like and temperature-like signals (i.e. $\sqrt{e_u^{-2}}$ and $\sqrt{e_T^{-2}}$) are read on R.M.S. meters with the function switch setting at A and B respectively on the second signal conditioner. To obtain actual values of the fluctuating quantities, the meter readings are divided by the gain setting.

The velocity-temperature correlation signal $\overline{ut}$, is obtained by addition and subtraction of the two individual signals with the function switch at the (A+B) and (A-B) settings respectively. The correlation is derived as explained below, where G_1 and G_2 are the gains for the respective signals.

$$(G_1A)^2 + (G_2B)^2 + 2G_1G_2\,AB = (G_1A + G_2B)^2 \qquad (2.4.1)$$

$$(G_1A)^2 + (G_2B)^2 - 2G_1G_2\,AB = (G_1A - G_2B)^2 \quad . \qquad (2.4.2)$$

Substracting (2.4.2) from (2.4.1) yields $\overline{AB}$ correlation as

$$\overline{AB} = \frac{(G_1A + G_2B)^2 - (G_1A - G_2B)^2}{4G_1G_2} \quad . \qquad (2.4.3)$$

The mean temperature signals recorded by DC voltmeters were converted to the actual temperatures using the linear calibration given in equation (2.2.4). Decomposing the instantaneous values into mean and fluctuating components and averaging yields

$$\overline{T} = Ao + A_2 \overline{E_T} \tag{2.4.4}$$

where Ao and A_2 are determined from the calibration data. The R.M.S. temperature is given by

$$\sqrt{t^2} = \lim_{\tau\to\infty} \frac{1}{\tau} \left[\int_0^{\tau} (T-\bar{T})^2 d\tau \right]^{1/2} . \tag{2.4.5}$$

Substituting equations (2.2.4) and (2.4.4) into equation (2.4.5) and simplifying yields

$$\sqrt{t^2} = A_2 \sqrt{e_T^2} . \tag{2.4.6}$$

The velocity calibration relation in non-dimensionalized and temperature independent form is given in equation (2.2.3), where the constants are determined from the calibration data. The equation (2.2.3) can be subjected to the Reynolds decomposition method to find the actual mean velocity at any location in the flow from the recorded velocity-like signals, where from the equation (2.2.2) the Nusselt number can be written as

$$N_u = \frac{E_u^2 R_w}{(R_w+51)^2 \pi \ell (T_w-T) k} \tag{2.4.7}$$

where(R_w+51) is the sum of the active arm of the bridge and resistance of the line at the operating temperature. Mahmood Ahmad (29) worked out a series of mathematical analysis and proved that the measured voltages such as $\overline{E_u}$, $\overline{e_u^2}$, $\overline{E_T}$, $\overline{e_T^2}$, $\overline{e_u e_T}$, correspond to $\overline{U}$, $\overline{u^2}$, $\overline{\Delta T}$, $\overline{t^2}$ and $\overline{ut}$.

2.5 Measurements

The hot wire probe used for turbulence measurements is illustrated in Figure (2.5). It consists of two parallel wires of 5 μ diameter tungsten with gold plated ends and a length to diameter ratio of 250.

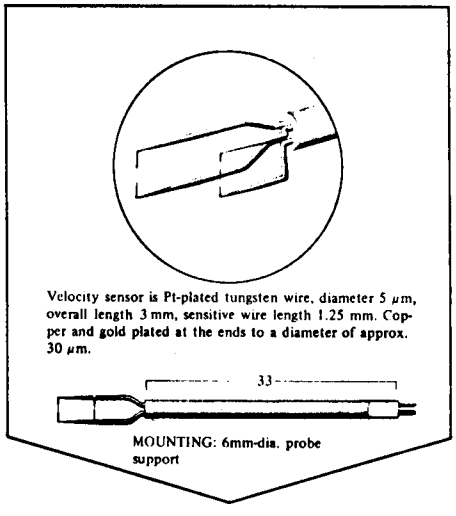

Figure (2-5) Probe

The probe is designed and manufactured by DISA Electronics. A 90° bent holder was used to hold the probe in position. One wire was used to measure velocity and was operated with an overheat ratio of 1.75. The other wire operated at much lower overheat and was used as a resistance thermometer. The position of the probe was such that the velocity wire was above the temperature wire to avoid the effect of the hot wake on temperature measurements.

The schematic of the data acquisition system is shown in Figure(2-6). The anemometer bridge output voltages were averaged for 100 seconds with an integrating digital voltmeter (DISA 55D31) to obtain the mean temperature and velocity-like signals. The same two signals were input to the R.M.S. voltmeter (DISA 55D35) via the signal conditioners (DISA 55D26) and averaged for 100 seconds to obtain R.M.S. velocity-like and temperature-like signals Because of the low frequencies which characterized this investigation (5-50H it was necessary to ensemble average successive readings for 10-20 minutes to obtain stable averages (within 5%).

High frequency noise was filtered by passing the signals through the signal conditioners at 1KHz low pass. Velocity and temperature signals were added and subtracted before squaring and averaging to obtain the velocity-temperature correlation. As two signals were being added and subtracted, it was necessary to keep both signals in approximately the same order of magnitude. Consequently the velocity signal was amplified by varyi the gain from 2-10 depending upon the probe position in the flow. The veloci temperature and the added and subtracted signals were obtained by changing the function switch on the other signal conditioner.

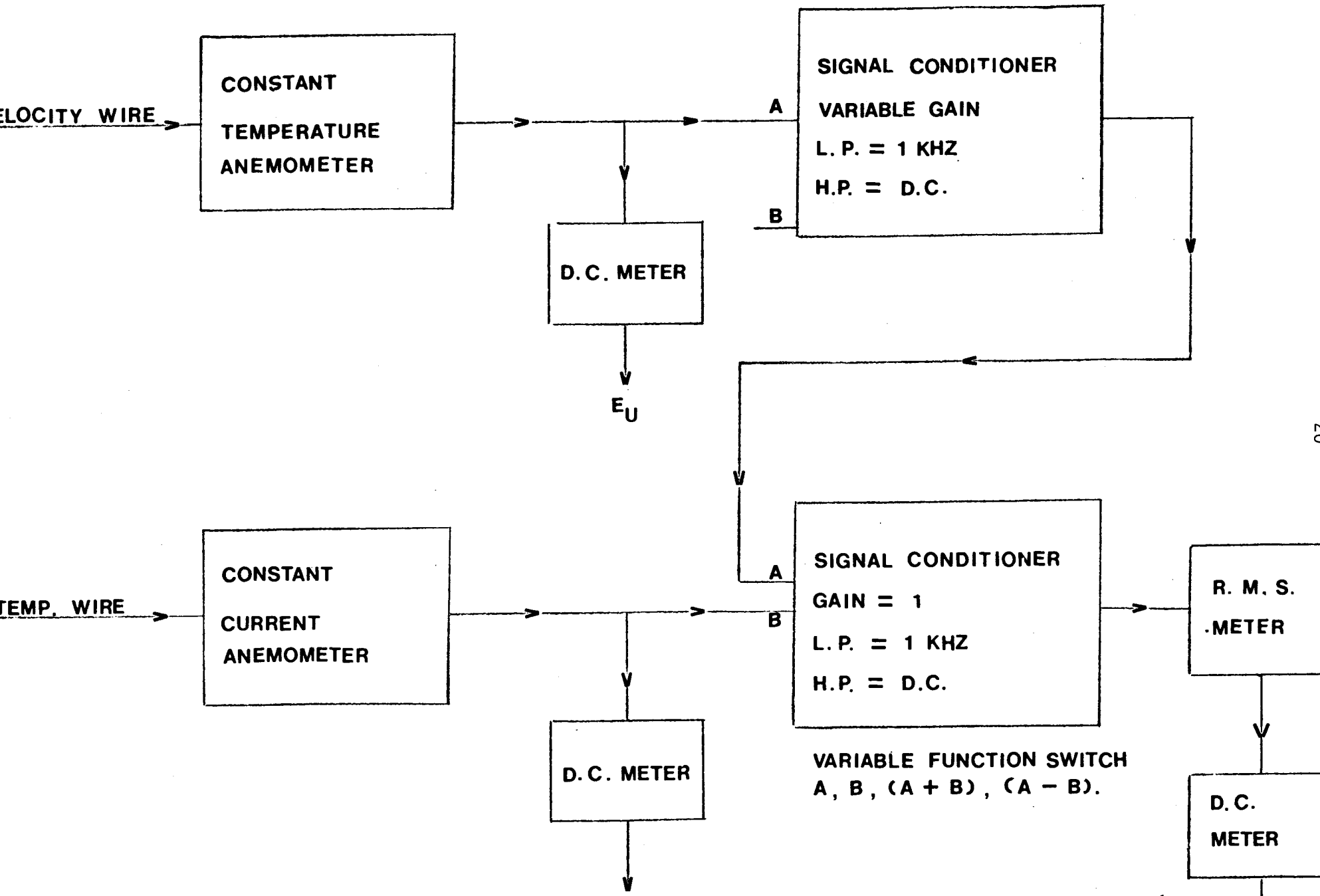
ELOCITY WIRE
CONSTANT
TEMPERATURE
ANEMOMETER
D.C. METER
E_U
A
B
SIGNAL CONDITIONER
VARIABLE GAIN
L.P. = 1 KHZ
H.P. = D.C.
TEMP. WIRE
CONSTANT
CURRENT
ANEMOMETER
D.C. METER
A
B
SIGNAL CONDITIONER
GAIN = 1
L.P. = 1 KHZ
H.P. = D.C.
VARIABLE FUNCTION SWITCH
A, B, (A + B), (A − B).
R.M.S.
METER
D.C.
METER

3. Results and Discussion

3.1 Test Conditions

The experiment was conducted at Froude numbers of 22.06 and 10.74 where Froude number is defined as

$$F_r = \left(\frac{\Delta\rho}{\rho_o}\frac{gD}{u^2}\right)^{-1/2} . \qquad (3.1.1)$$

The corresponding length scales, $L\left(\frac{M_o^{3/4}}{F_o^{1/2}}\right)$ were 0.66 and 0.32. Data were obtained at 1.0, 1.25 and 1.5 meters from the source, which corresponds to x/D values of 31.5, 39.4, 47.2, (D = 0.0318m). The test conditions are given in the following table.

Expt. No.	Q(CFH)	$T_{source}(^oK)$	$\bar{U}_E$(m/s)	$M_o\left(\frac{L^4}{T^2}\right)$	$F_o\left(\frac{L^4}{T^3}\right)$	F_r	$\xi(=x/L)$
1	600	483	9.63	73.5×10^{-3}	4.6×10^{-2}	22.06	1.5 1.9 2.3
2	300	563	5.62	25.0×10^{-3}	3.8×10^{-2}	10.74	3.1 3.9 4.7

The flow dominated by momentum corresponds to the parameter $\xi \leq 1.0$ defined by the jet equations , and the flow dominated by buoyancy corresponds to $\xi >> 1.0$ defined by the plume equations.

These experiments were conducted at values of the length scale (L) of 0.66 and 0.32. Hence jet-like flows should be observed at heights of 0.66 and 0.32m or less for the respective values of L, and plume-like flows should be observed at heights of 6.6 and 3.2 m or more for the respective values of L. Since these tests were conducted at heights of 1.0, 1.25 and 1.5 m, this study was limited to buoyant jet flows.

The ambient temperature data are shown in Figure 3.1. This figure shows that the maximum ambient temperature stratification is approximately

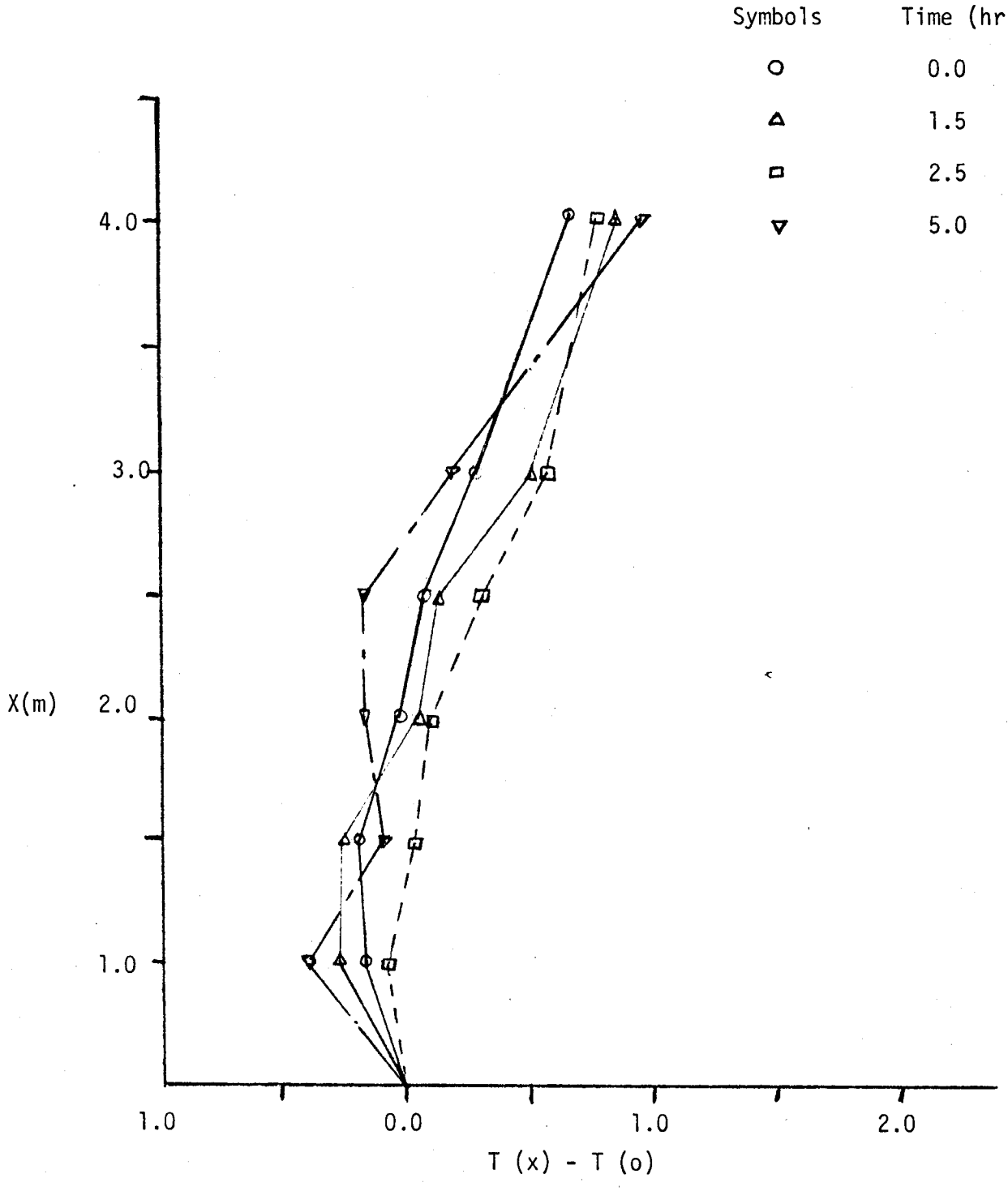

Figure 3.1 Ambient Temperature

0.75°F over the temperature range of these tests. Consequently, the modifications of the experimental structure eliminated the problems encountered by Beuther (2) and Ahmad (29).

The measured buoyancy flux at any plane normal to the mean flow can be used as a measure of flow stratification, since F_o is constant throughout the flow field. The total heat flux was measured at various vertical stations in the flow field. These were integrated and compared with the initial buoyancy F_o. The results are given in Figures (3.2) and (3.3) which show that the decrease in buoyancy for both test conditions does not exceed 4%.

3.2 Mean Centerline Data

Beuther et al. (11) have indicated that the mean centerline data for jets, plumes and buoyant jets are probably the most accurate because this is the region of least turbulence intensity. Figures (3.4) and (3.5) depict the mean velocity and temperature data respectively presented by Baker (9). In addition, those figures contain the analytical solution developed by Baker (9). The values for the horizontal asymptotes were obtained from existing jet data, and the plume asymptotes for both cases were obtained from the analytical solution. It appears from the centerline temperature data that a horizontal asymptote of 5.6 may fit the data better than the 5.95 value used by Baker (9). The scarcity of buoyant jet and plume mean velocity data are obvious from Figure (3.4).

The centerline velocity and temperature data from this investigation are shown in Figures (3.6) and (3.7) along with data of George,et al.(3), Ahmad (29), and Baker's (9) analytical solution. The agreement of all data and the analytical solutions are seen to be reasonable.

Symbol	x/L	x/D
○	1.5	31.5
□	1.9	39.4
△	2.3	47.2

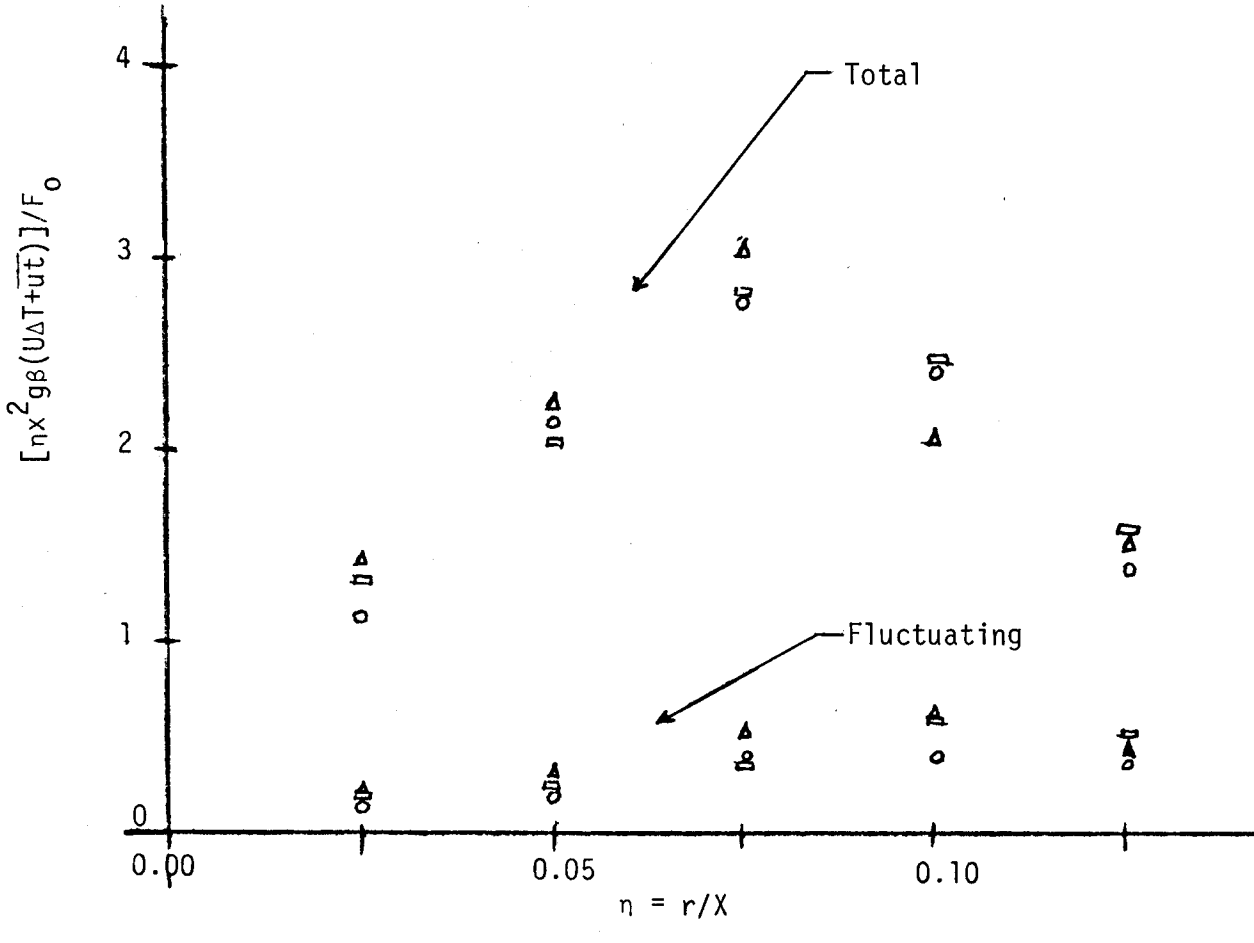

Figure 3.2 Buoyancy Flux
Froude No. 22.06, L = 0.66

Symbol	x/L	x/D
○	1.5	31.5
□	1.9	39.4
△	2.3	47.2

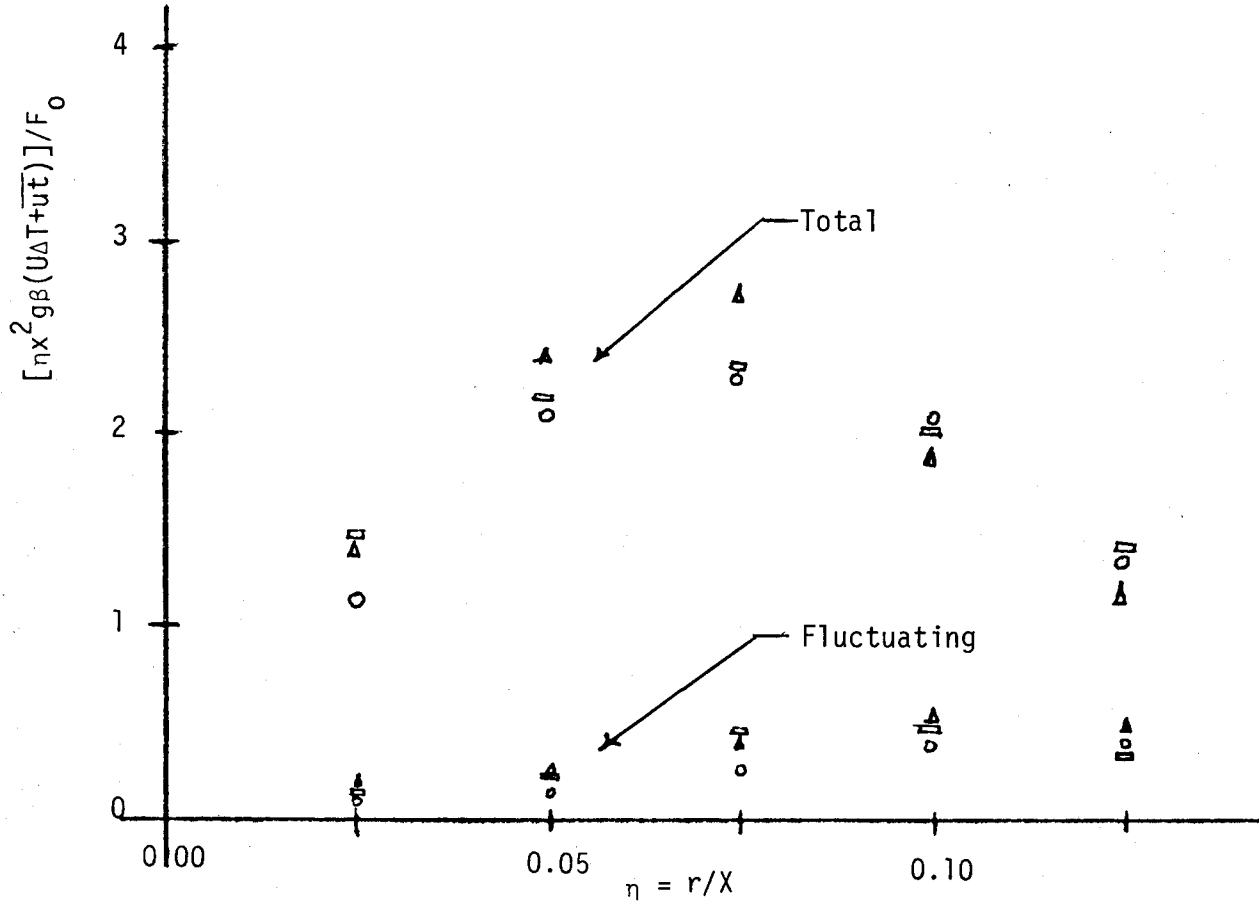

Figure 3.3 Buoyancy Flux
Froude No. 10.74, L = 0.32

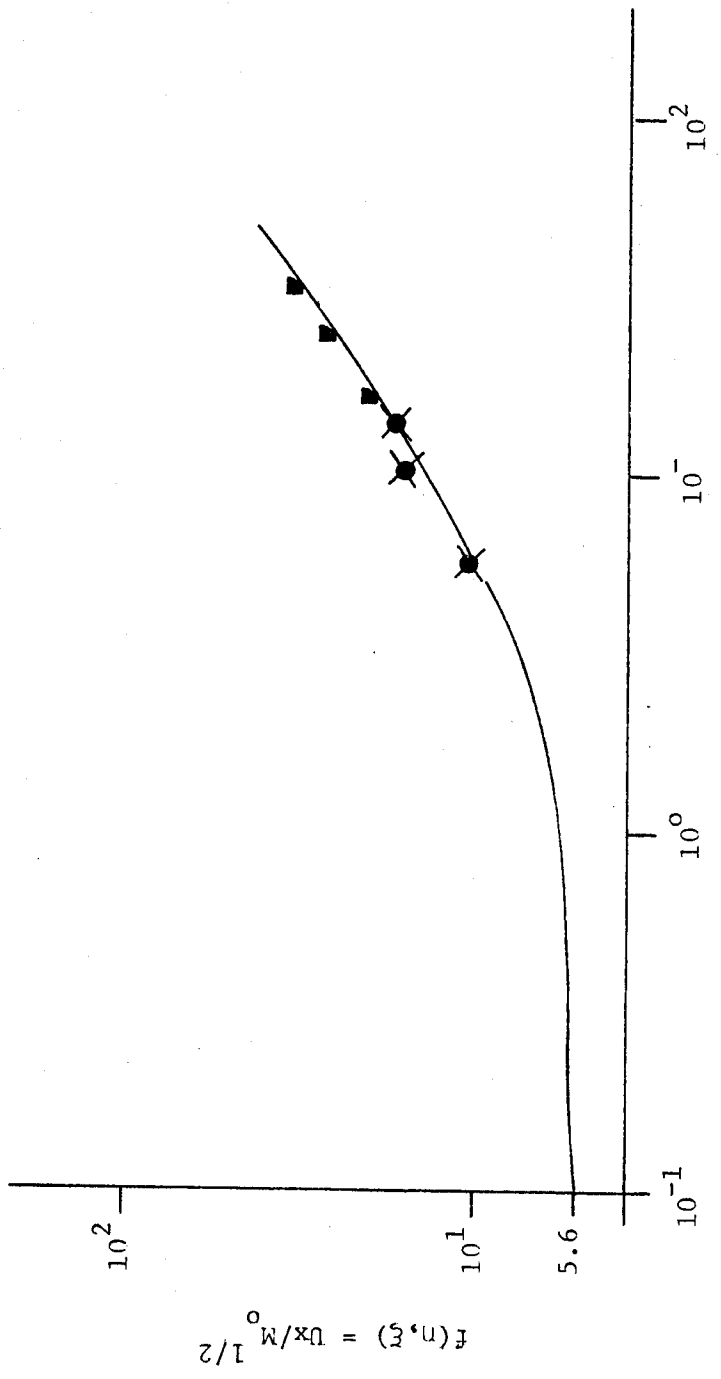

Figure 3.4 Comparison of calculated buoyant jet mean centerline velocity with data. ✕ - George, et al. (23). ◗ - Ahmad (44).

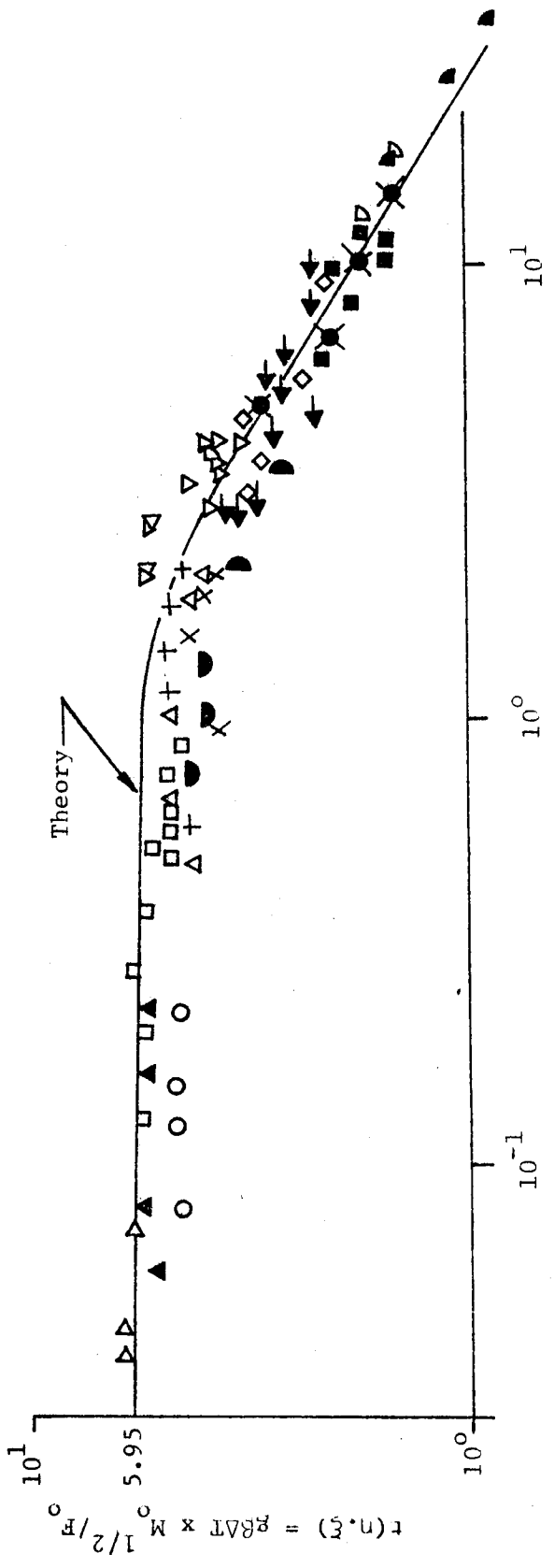

Figure 3.5 Comparison of calculated buoyant jet centerline temperature.

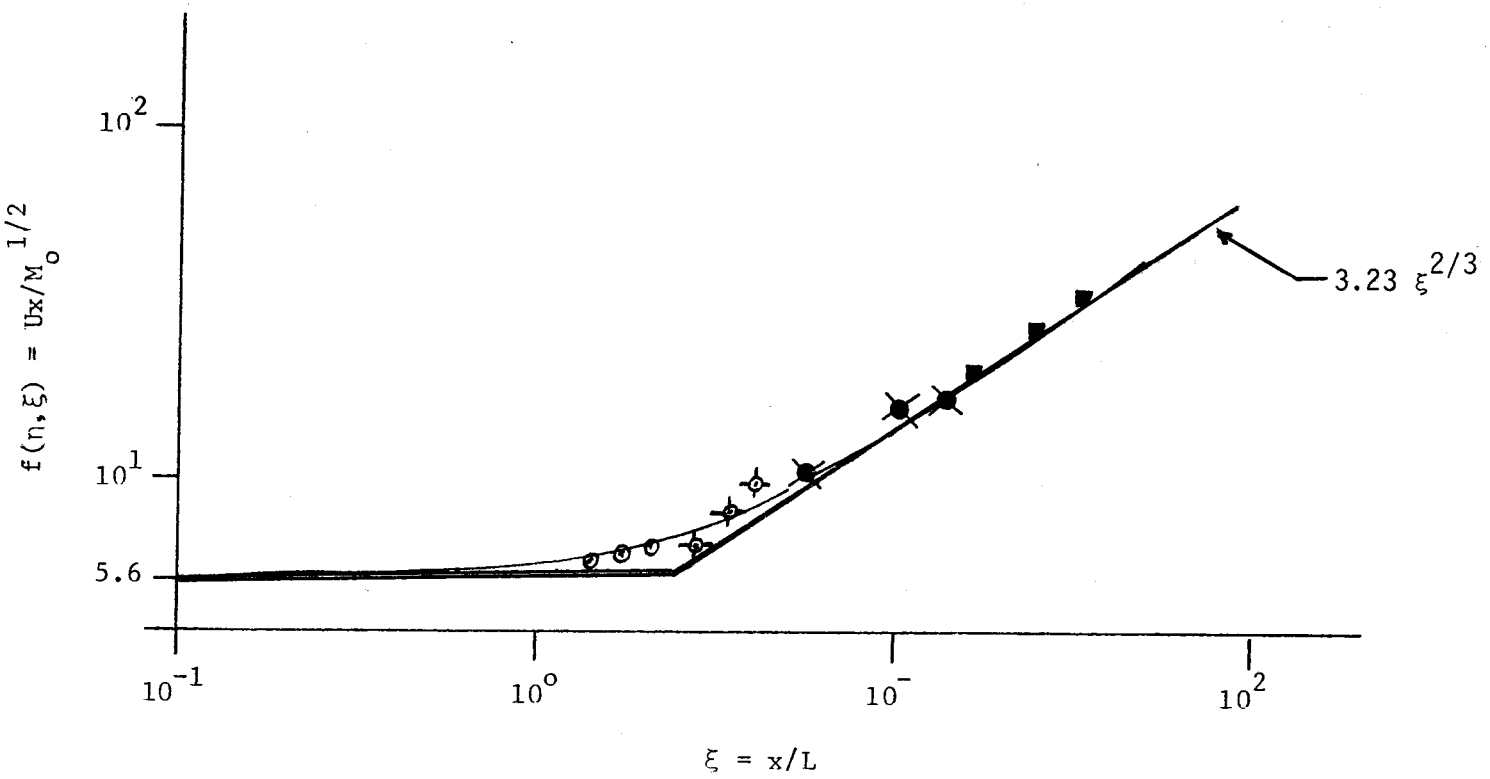

Figure 3.6 Comparison of calculated buoyant jet mean centerline velocity and asymptote.
- George, et al. (23). - Ahmad (44).
- Froude # 22.06, - Froude #10.74

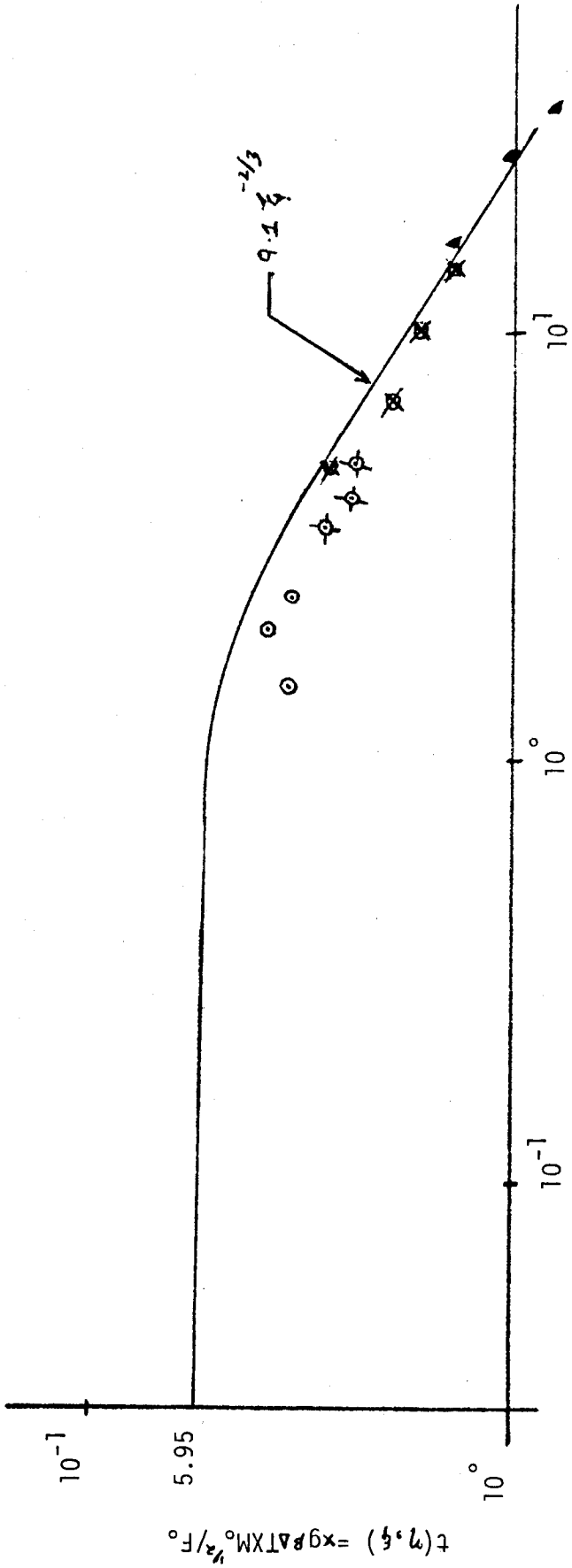

Figure 3.7 Buoyant Jet Centreline Temperature Data.

⊙ - Froude # 22.1, ⊙ - Froude # 10.7

⊠ - George et. al.(3) ◣ - Ahmad(29)

3.3 Mean Velocity and Temperature Profiles

The measured velocity profiles obtained for Froude number of 22.06 and L = 0.66 are shown in Figure (3.8). Data are presented for ξ values of 1.5, 1.9 and 2.3, all of which are within the buoyant jet domain. The measured jet velocity profile of Wygnanski (30) and the theoretical solutions of Baker (9) for ξ = o and 2.5 are also presented in this figure. The present data do not collapse, a result of which is consistent with the conclusion of Baker (9). Also these velocity data are higher than those of Wygnanski (30). Another result which is consistent with arguments of Baker (9) in which it is shown that the profile of Wygnanski (30) is too low because it fails to account for 50% of the mean momentum. For $r/x > 0.075$ the present data are lower than Baker's results. That is consistent with the fact that an eddy viscosity model over-predicts the mean profiles at the outer edge of the jet flow and hot wires underestimate the velocity in this region. This underestimate is a result of cross flow caused by high turbulence intensity. Figure (3.9) shows similar results for a Froude number of 10.74 and L = 0.32. The same trends can be observed as in Figure (3.8). To this author's knowledge the data from the present study are the only velocity data available in the transition flow region of the buoyant je

The measured mean temperature profiles are shown in Figures (3.10) and (3.11) for Froude numbers of 22.06 and 10.74 respectively. The empirical fi of George et al. (3) for a pure plume is also shown in these figures. The results of Baker show only modest differences in the temperature profiles, and the data of George et al. are considered representative of the plume temperature profiles. At the outer edge the hot wire overestimates T_∞ by 1.5° or less as measured by the thermocouple. The data are adjusted to compensate for this difference. Within experimental error the buoyant jet, hot jet and plume temperature profiles appear to be identical.

Symbol	x/L	x/D
o	1.5	31.5
□	1.9	39.4
△	2.3	47.2

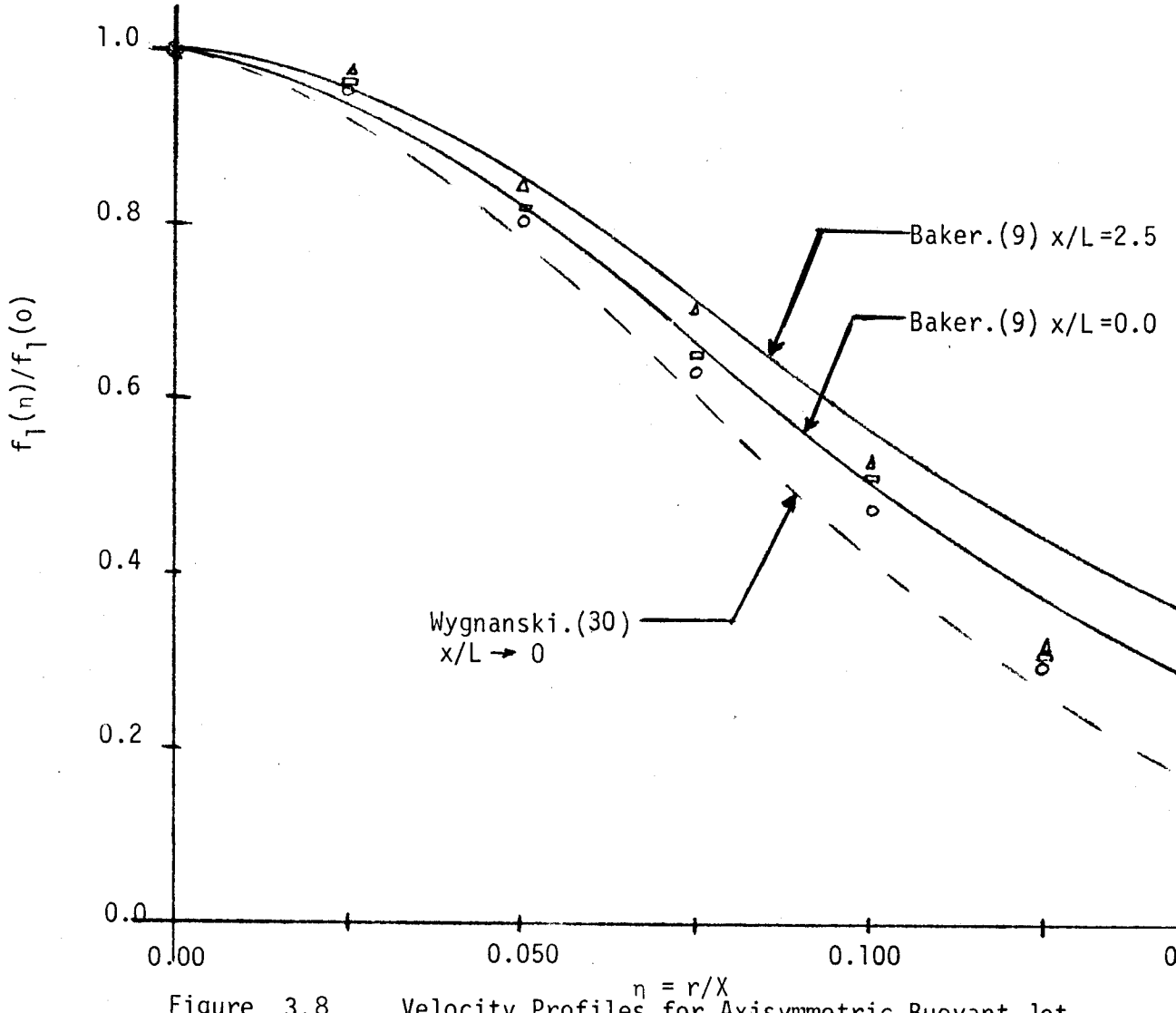

Figure 3.8 Velocity Profiles for Axisymmetric Buoyant Jet.

Froude No. 22.06 , L = 0.66

Symbol	x/L	x/D
o	3.1	31.5
□	3.9	39.4
Δ	4.7	47.2

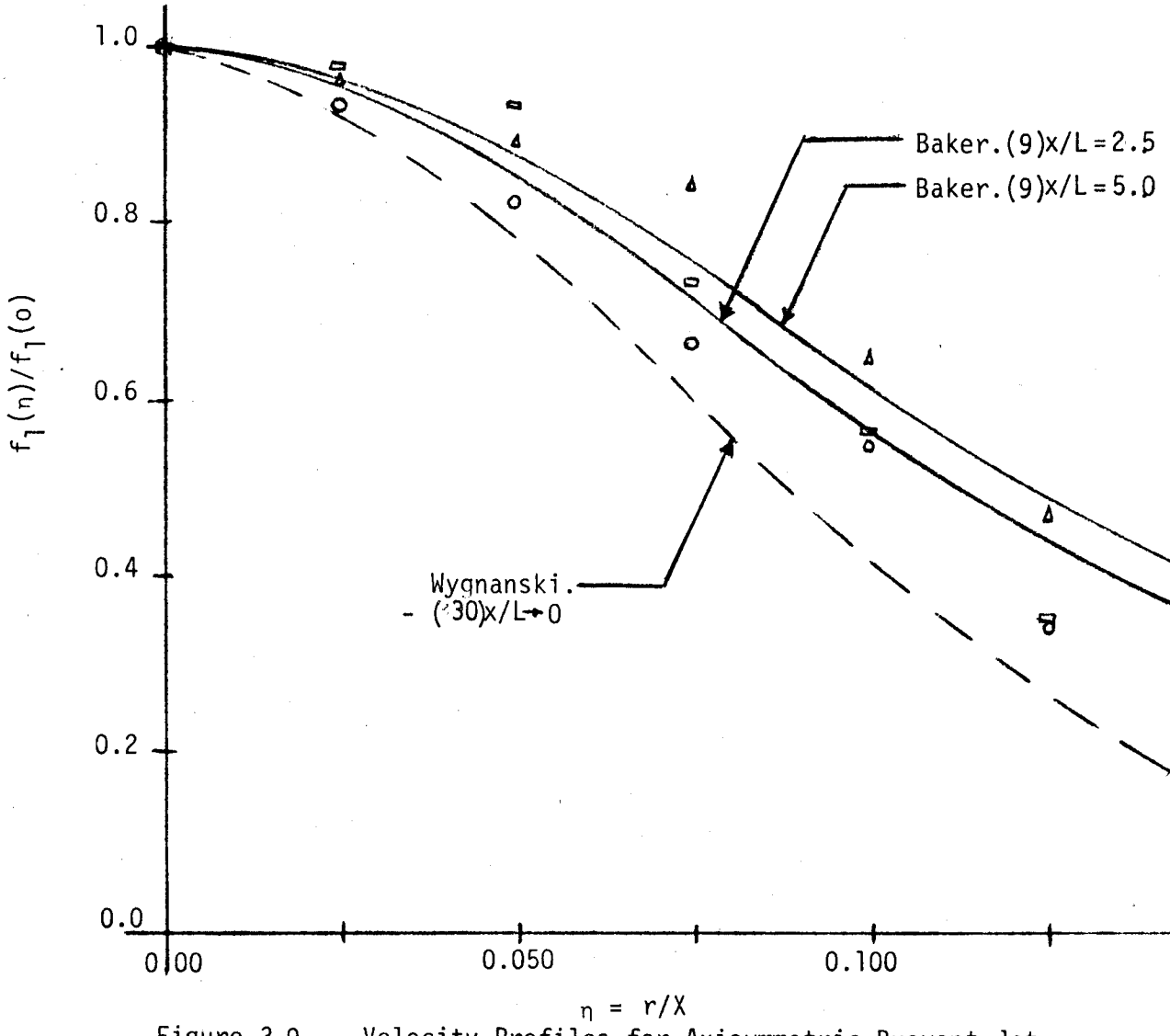

Figure 3.9 Velocity Profiles for Axisymmetric Buoyant Jet

Froude No. 10.74, L = 0.32

Symbol	x/L	X/D
○	1.5	31.5
□	1.9	39.4
△	2.3	47.2

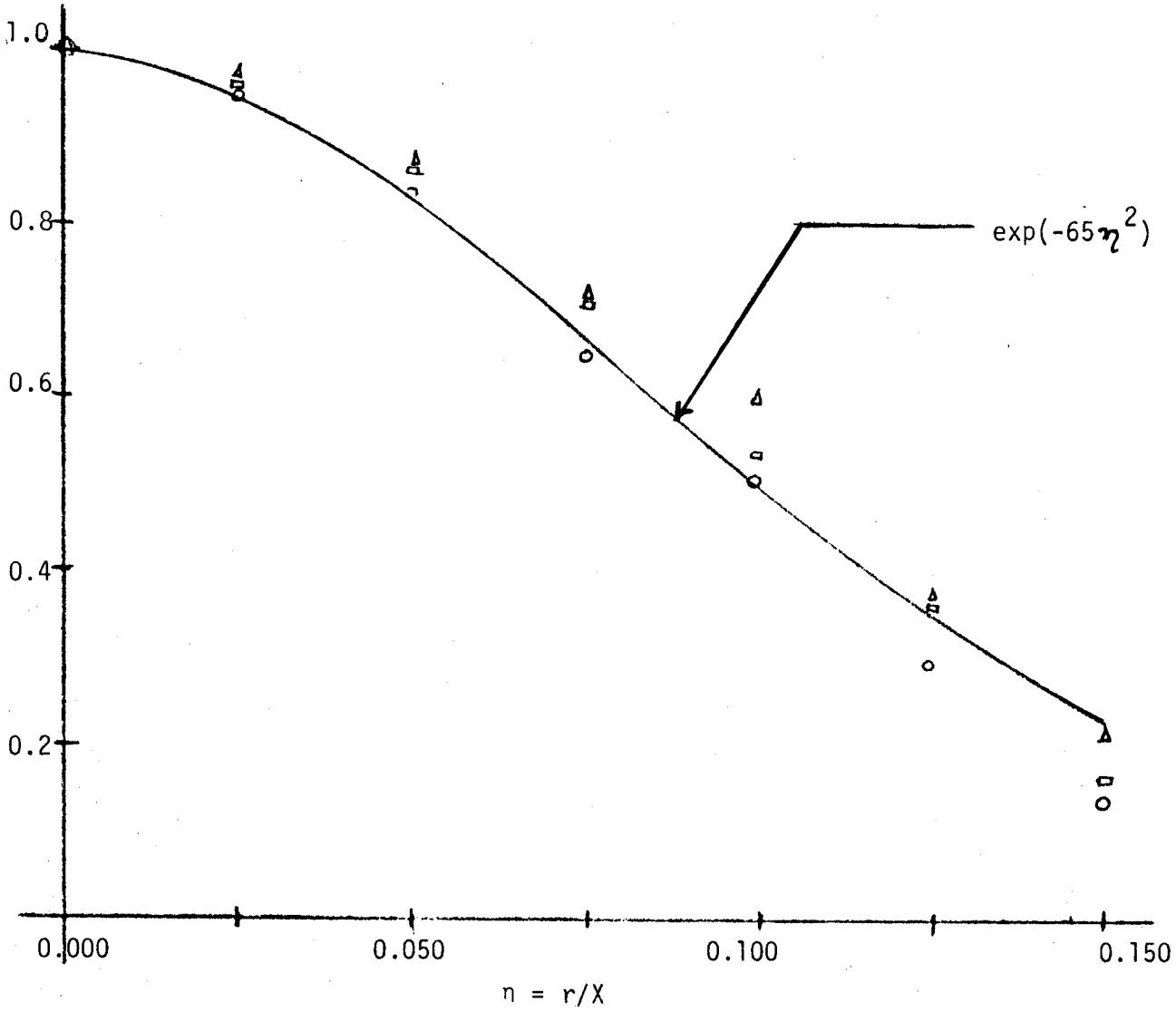

Figure 3.10 Temperature Profiles for Axisymmetric Buoyant Jet

Froude No. 22.06 , L = 0.66

Symbol	x/L	x/D
o	3.1	31.5
□	3.9	39.4
Δ	4.7	47.2

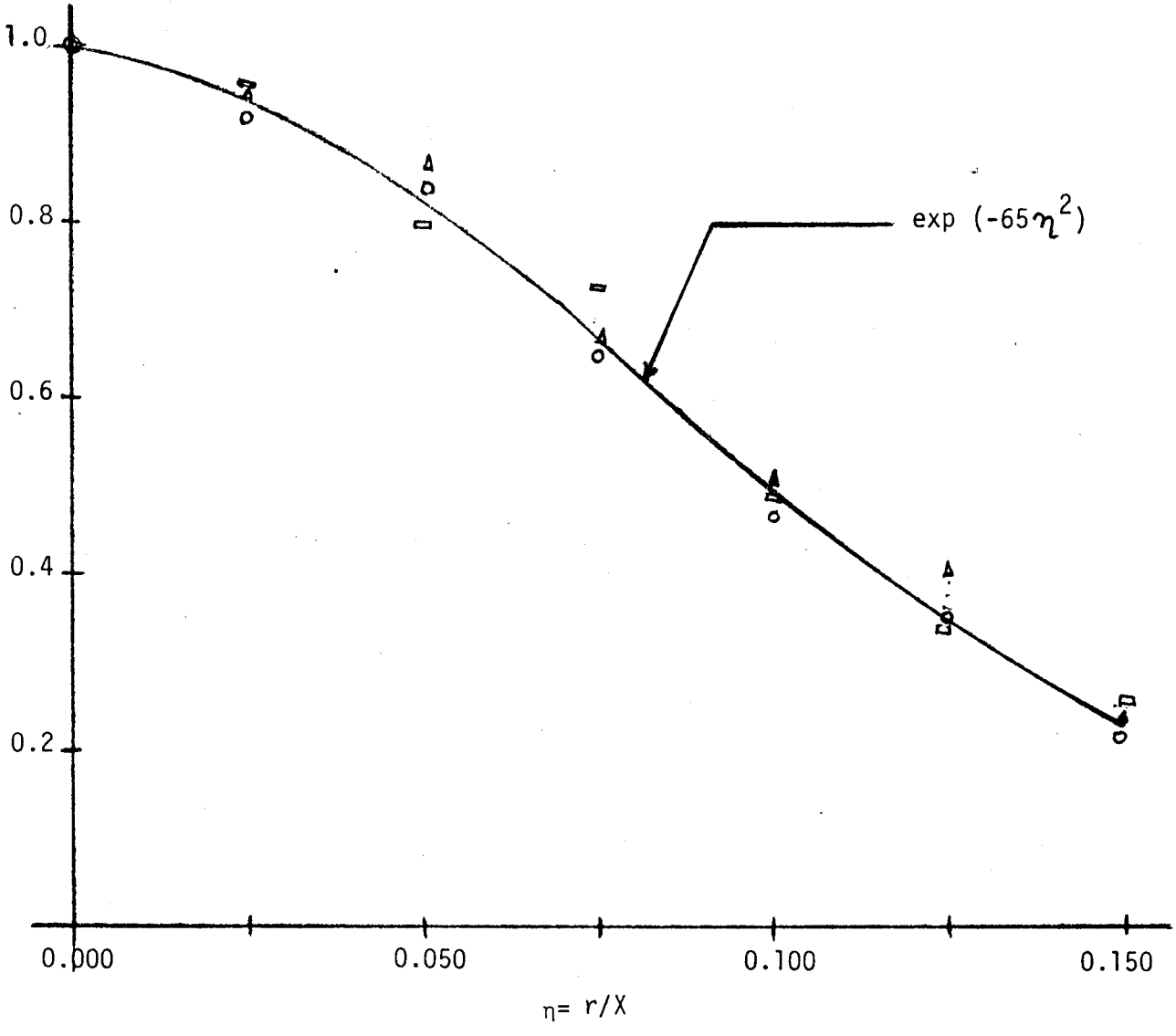

Figure 3.11 Temperature Profiles for Axisymmetric Buoyant Jet
Froude No. 10.74, L = 0.32

3.4 Measurements of Fluctuating Quantities

The R.M.S. values of fluctuating velocity and temperature are shown in Figures (3.12) through (3.15). Jet turbulent velocity intensity ($\xi \to 0$) measured by Wygnanski is approximately 20%. The measured values at buoyant jet turbulent velocity intensities shown in Figures (3.12) and (3.13) range from 0.25 to 0.40. Similar data for the plume vary from 25% to 30%. These results imply that a time delay occurs between the point at which buoyancy effects begin to increase turbulence intensities and the point at which dissipation begins to degrade the turbulence. Consequently, the plume equilibrium has not been established. The fluctuating temperature results given in Figures (3.14) and (3.15) show trends similar to the temperature data of Figures (3.10) and (3.11).

The measured buoyant jet velocity-temperature correlation coefficients are shown in Figures (3.16) and (3.17). For a jet this coefficient is approximately 0.2, and for a plume this coefficient is approximately 0.65. The measured values for the buoyant jet lie well within the values of a jet and a plume. The variation of the correlation coefficient with η is explained by the radial momentum transport of hot fluid and its contribution to the outer edge of buoyancy dominated flows. In flows of this type the center region mechanical turbulence still dominates the center region.

Symbol	x/L	x/D
o	1.5	31.5
□	1.9	39.4
Δ	2.3	47.2

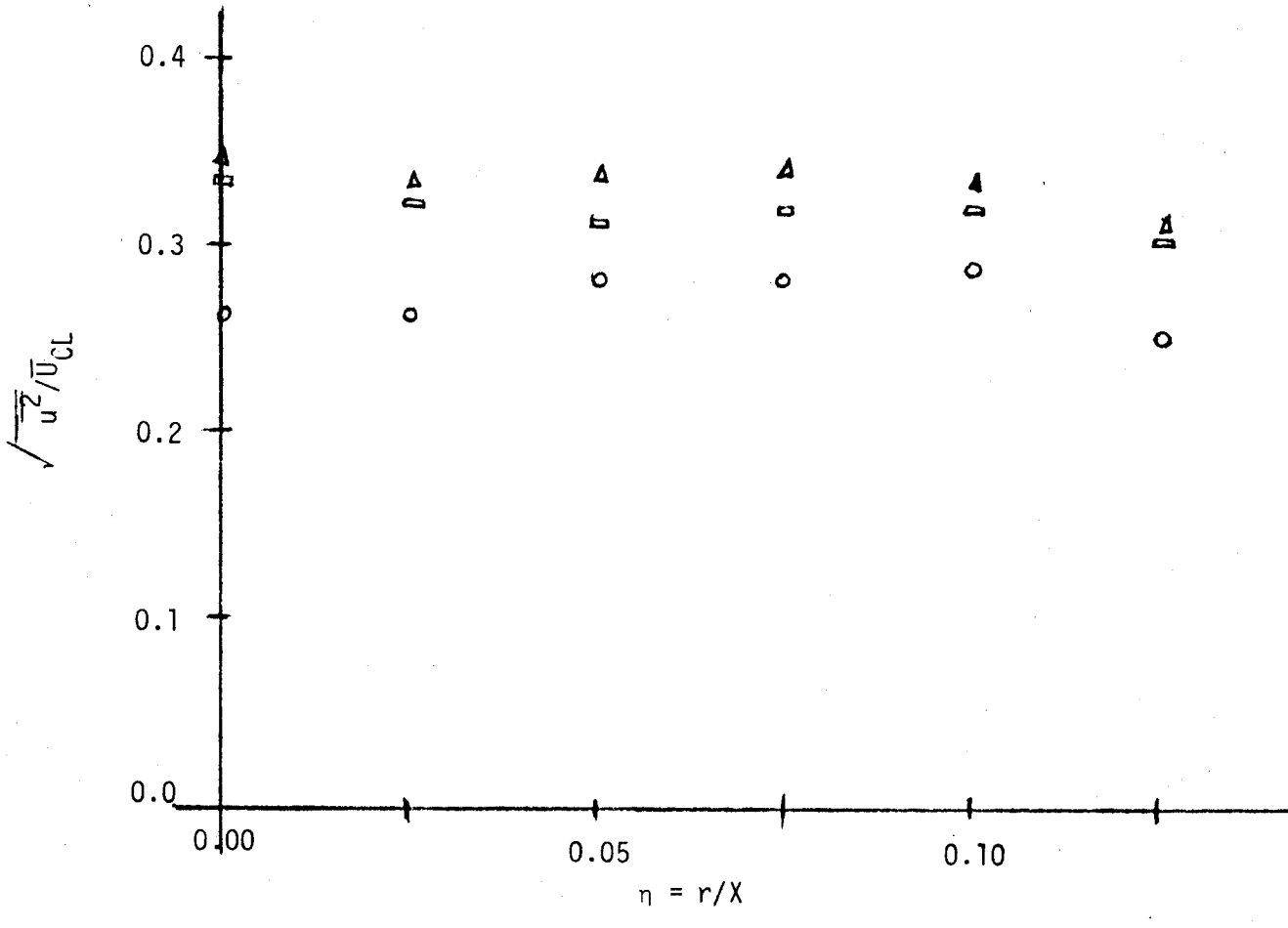

Figure 3.12 Intensity of Velocity Fluctuations
Froude No. 22.06, L = 0.66

Symbol	X/L	x/D
○	1.5	31.5
□	1.9	39.4
△	2.3	47.2

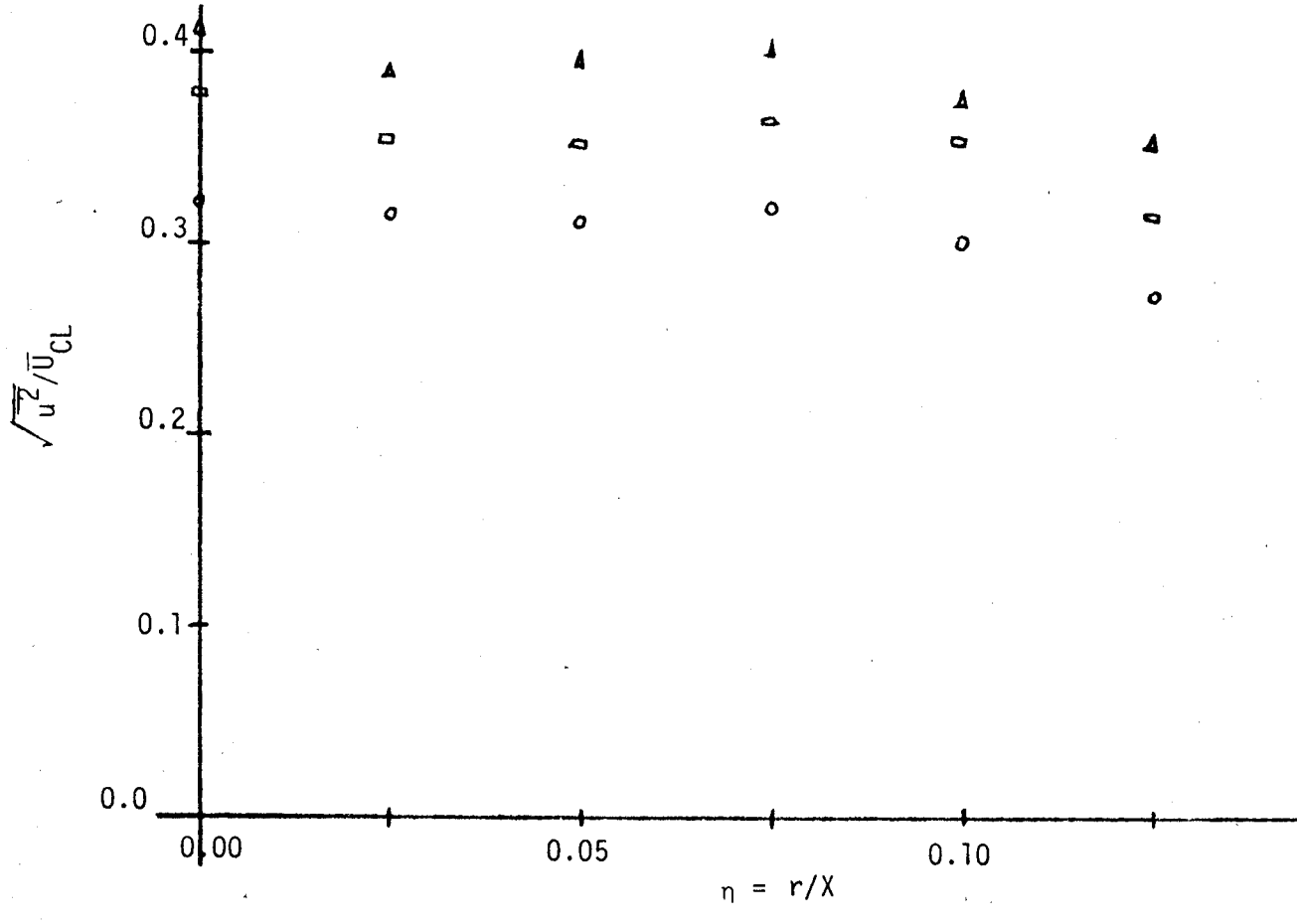

Figure 3.13 Intensity of Velocity Fluctuations
Froude No.10.74, L = 0.32

Symbol	x/L	x/D
O	1.5	31.5
□	1.9	39.4
△	2.3	47.2

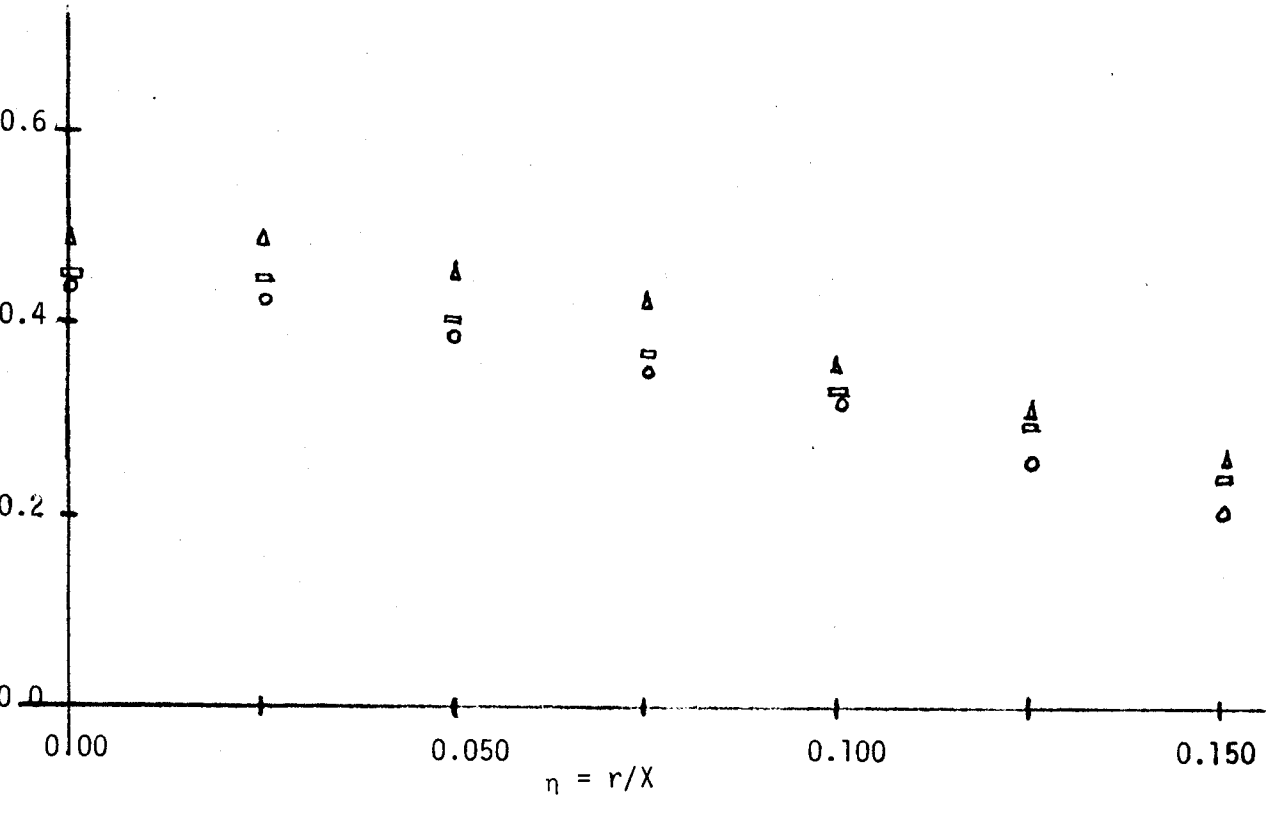

Figure 3.14 Intensity of Temperature Fluctuations
Froude No. 22.06, L = 0.66

Symbol	x/L	x/D
○	1.5	31.5
□	1.9	39.4
△	2.3	47.2

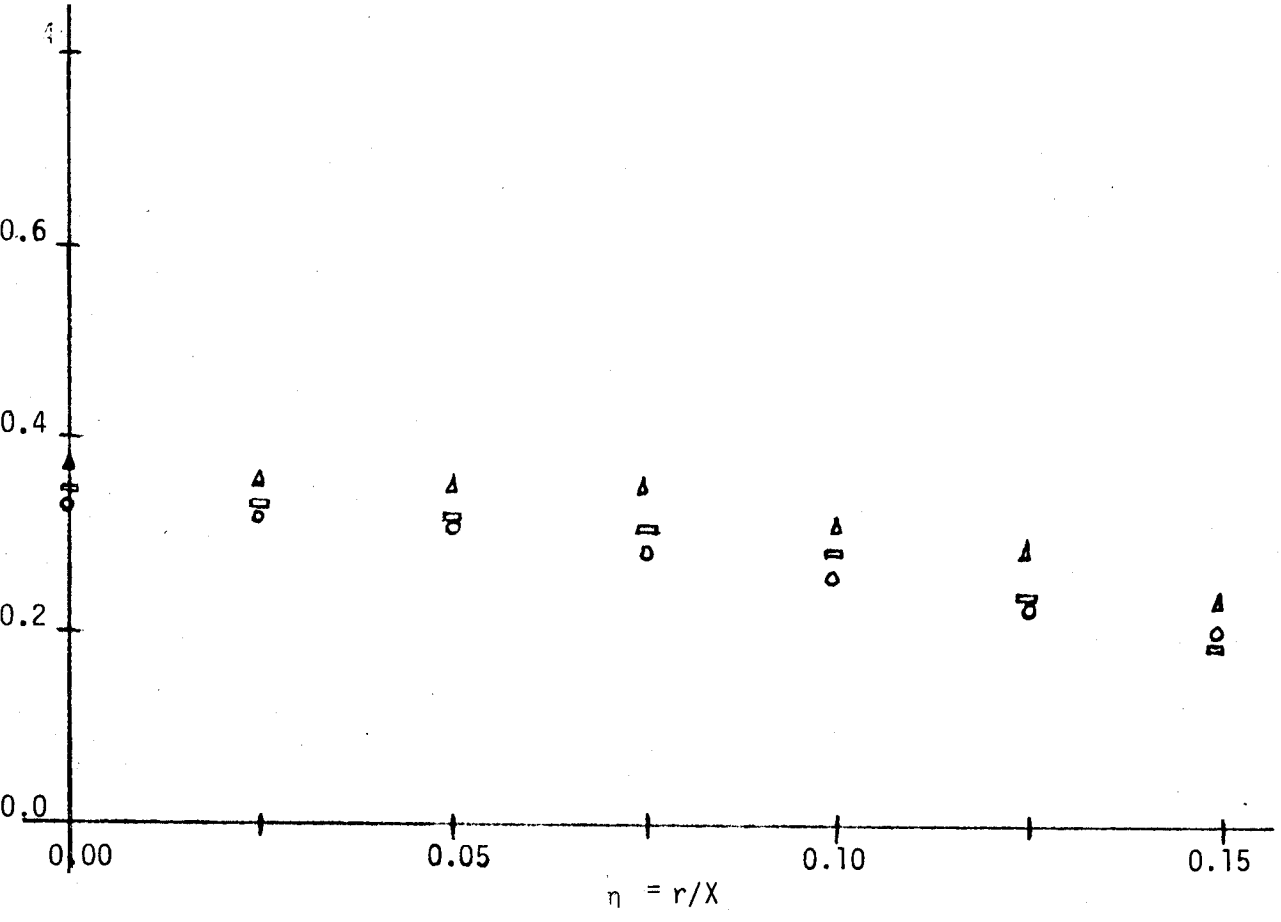

Figure 3.15 Intensity of Temperature Fluctuations

Froude No. 10.74, L = 0.32

Symbol	x/L	x/D
○	1.5	31.5
□	1.9	39.4
△	2.3	47.2

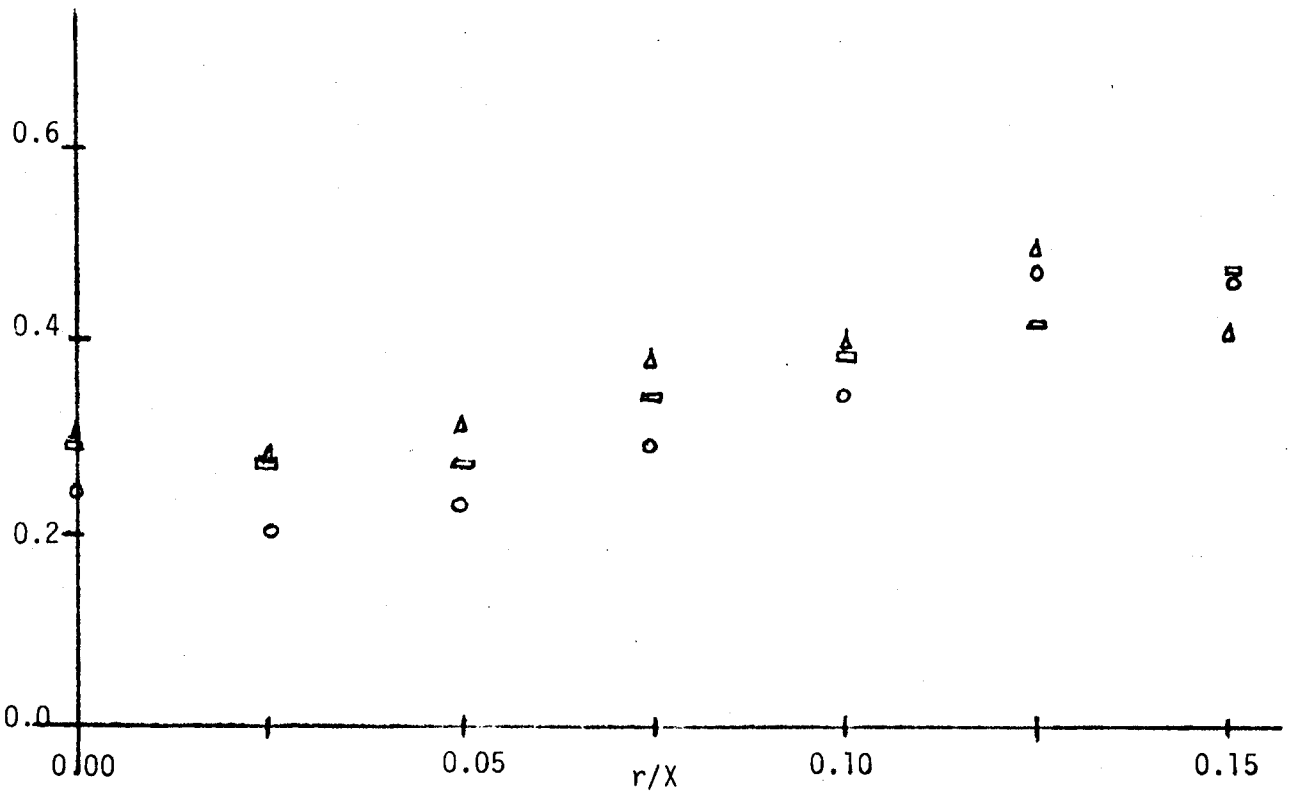

Figure 3.16 The Velocity-Temperature Correlation Coefficient

Froude No. 22.06, L = 0.66

Symbol	x/L	x/D
○	3.1	31.5
□	3.9	39.4
△	4.7	47.2

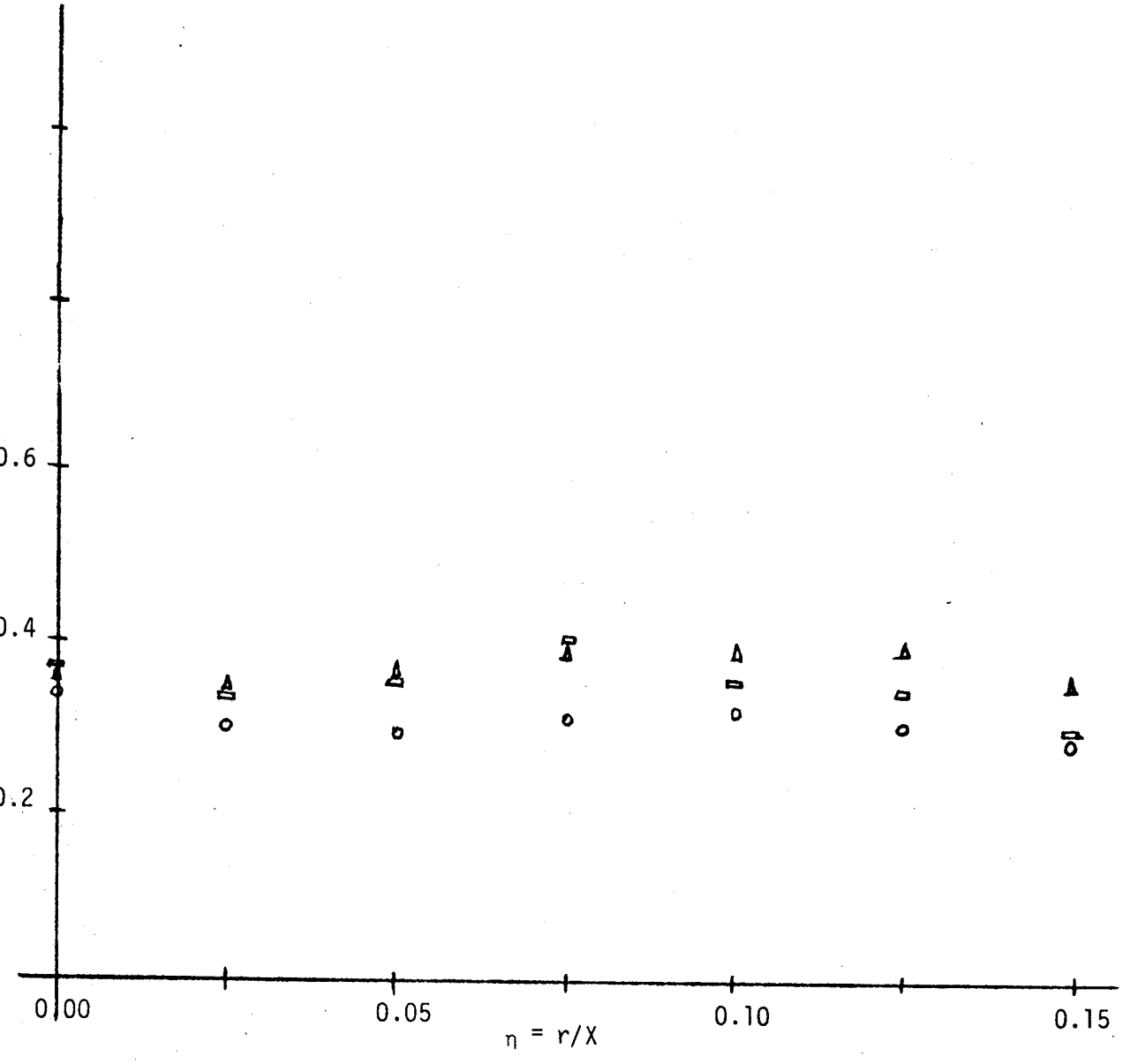

Figure 3.17 The Velocity-Temperature Correlation Coefficient
Froude No.10.74, L = 0.32

4. Summary and Conclusions

The objective of this thesis was a detailed study of the axisymmetric buoyant jet in a neutrally stable environment. During this study it was sho that the ambient stratification encountered by Beuther (2) and Ahmad (29) could be eliminated. Consequently a 96 to 98.5% conservation was achieved.

The centerline velocity data are in good agreement with the theory of Baker (9). The centerline temperature data are in good agreement with existing data of this type and indicate that Hinze's (22) value of 5.6 for the jet centerline asymptote may be better than the 5.95 value proposed by Baker (9). Theoretically this implies a turbulent Prandtl number of 1.0 since the accepted value of the centerline jet velocity asymptote is also 5.6.

The near jet velocity profile supports the conclusion of Baker (9) that the data of Wygnanski (30) are low and fail to account for 50% of the momentum. In addition the measured velocity profiles for the buoyant jet support the trends predicted by Baker (9) and are in reasonable agreement with Baker's predictions. Within experimental error the hot jet, buoyant jet, and plume mean temperature profiles were identical; another result predicted by Baker's theoretical study.

Lastly, the turbulence intensities in the buoyant jet region are greate than those encountered in either the pure jet or plume. This implies that a time delay occurs between the point at which buoyancy effects begin to increase the turbulence intensity and the point at which dissipation begins to degrade the turbulence. Theoretically this implies that in high order models the buoyancy induced turbulence term would be controlled by a lower order ξ form than the turbulence dissipation term. This result warrants a more detailed study to establish the relation between ξ and the buoyance induced turbulence and turbulence dissipation.

REFERENCES

1. Baker, C.B., Taulbee, D.B., George, W.K. Eddy Viscosity Calculations of Turbulent Buoyant Plumes , Joint ASME/AIChE 18th National Heat Transfer Conference, San Diego, Ca. 1979.

2. Beuther, P.D., Experimental Investigation of the Axisymmetric Turbulent Buoyant Plume , Ph.D. Dissertation submitted to the Graduate School of State University of New York at Buffalo, 1980.

3. George, W.K., Alpert, R.L. and Tamanini, F. Turbulence Measurements in an Axisymmetric Buoyant Plume , Int. J. Heat Mass Trans. V.20, 1145-1154, 1977.

4. Madni, I.K. and Pletcher, R.H. Predictions of Turbulent Forced Plumes Issuing Vertically with Stratified or Uniform Ambients , Trans. ASME, J. Heat Transfer, 99-104, 1977.

5. Nakagome, H. and Hirata, M. The Structure of Turbulent Diffusion in an Axisymmetric Thermal Plume , 9th Int. Conf. for Heat and Mass Trans. Inter. Seminar, Spalding, D., ed. V. 1, 361-372, Hemisphere Publishing Corp., Dukrovnik, Yugoslavia, 1976.

6. Rouse, H., Yih, C.S. and Humphreys, H.W. Gravitational Convection from a Boundary Source , Tellus 4, 201, 1952.

7. Taylor, G.I., Dynamics of a Mass of Hot Gas Rising in Air , U.S. Atomic Energy Commission, MDDC, 919, LADC 276, 1945.

8. Zel'dovich, Ya. B., Limiting Laws for Turbulent Flows in Free Convection , zh, eksp. Theoret. Fig. 7(12), 1463, 1937.

REFERENCES

9. Baker, C.B., An Analysis of the Turbulent Buoyant Jet , A Ph.D. Dissertation. The Pennsylvania State University, May, 1980.

10. Batchelor, G.K., Heat Convection and Buoyancy Effects in Fluids , Q. J.l.R. Met. Soc. 80, 334-358, 1954.

11. Beuther, P.D., Capp, S.P. and George, W.K. Momentum and Temperature Balance Measurements in an Axisymmetric Turbulent Plume. Joint ASME/AIChE 18th Nat. Heat Trans. Conf., San Diego, Ca. 1979.

12. Hamilton, C.M. and George, W.K. Eddy Viscosity Calculations for Turbulent Buoyant Plumes , Bull. Amer. Phys. Soc., Series II, V. 21, No. 10, 1225, 1976.

13. Morton, B.R., Taylor, G.I. and Turner, D.S. Turbulent Gravitational Convection from Maintained and Instantaneous Source , Proc. R. Soc. 234A, 1-23, 1956.

14. Rao, V.K. and Brzuztowski, T.A. Preliminary Hot-Wire Measurements in Free Convection Zones over Model Fires , Combust. Sci. Tech. 7, 171-180, 1969.

15. Schmidt, W.Z., Turbulent Propagation of a Stream of Heated Air , Z. Agnew. Math. Mech. 21, 265-351, 1941.

16. Yih, C.S. Turbulent Buoyant Plumes , The Physics of Fluids, 20, 8, 1234-1237, 1977.

REFERENCES

17. Tol mein, W., Benechnung Turbulenter Auxbreitunsvorgange, Zamm 6, 468-478, 1926.

18. Gortler, H., Berechnung von Aufgaben der Freien Turbulenz auf Grund eines neuen Naherungsansatzes, Zamm 22, 244-254, 1942.

19. Zimm, W., Uber die Strommungsvorgange in Frein Luftstrah, BDI-Forschungsheft, 234, 1921.

20. Ruden, P., Turbulente Aushbeitungim Freistrahl Naturwissenschaften 21, 375-378, 1933.

21. Reichardt, H., Gesetzma Bikeiten der freien Turbulenz, VDI-Forschungsheft 4.4, 1942.

22. Hinze, D.O. and van der Hegge Zignen, B. G., Transfer of Heat and Matter in the Turbulent Mixing Zone of an Axially Symmetrical Jet, Applied Scientific Research, Vol. A1, 435-461, 1949.

23. Corrsin, S. and Uberoi, M. S., Further Experiments of the Flow and Heat Transfer in a Heated Turbulent Jet, NACA Report No. 998, 1950.

24. Abraham, G., Jet Diffusion in Stagnant Ambient Fluid, Delft Hydraulics Laboratory Report No. 29, Delft, The Netherlands, 1963.

25. Kotsovinos, N. E., Dilution in a Vertical Round Buoyant Jet, Proc. ASCE, J. Hyd. Div., 104, 795-798, 1978.

26. Ryskiewich, B.S. and Hafetz, L., An Experimental Study of the Surface Effect on a Buoyant Jet, General Dynamics, Electric Boat Division, Report No. U440-74-103, Groton, Conn., 1975.

REFERENCES

27. Pryputniewicz, R.J., An Experimental Study of the Free Surface Effects on a Submerged Vertical Buoyant Jet, M.S. Thesis, University of Connecticut, 1974.

28. List, E. J. and Imerger, J., Turbulent Entrainment in Buoyant Jet and Plumes, Proc. ASCE, J. Hyd. Div., 99, 1416-1474, 1973.

29. Ahmad, M., Further Studies on the Turbulent Axisymmetric Buoyant Plume, M.S. Thesis, Department of Mechanical Engineering, State University of New York at Buffalo, Buffalo, NY, May 1980.

30. Wygnanski, I. and Fiedler, H. E., Some Measurements in Self-Preserving Jets, J. Fluid Mech., Vol. 38, Pt. 3, 577-612, 1969.